*Geophys. J. R. astr. Soc.* (1979) 57, 397–429

# $P_n$ anisotropy studies in northern Britain and the eastern and western United States

David Bamford, Martin Jentsch and Claus Prodehl

*Geophysical Institute, University of Karlsruhe*

Received 1978 October 2; in original form 1978 August 16

**Summary**. Available seismic refraction data from three different continental areas, northern Britain and the eastern and western United States, has been studied for possible $P_n$ velocity anisotropy using the methods described by Bamford. There are various deficiencies in the time–distance data used in each case but, while the uppermost mantle beneath northern Britain and the eastern United States seems to be isotropic within the limits of measurement error, there is a small but significant anisotropy beneath the western United States.

Both the amount (up to 3 per cent) and the direction (70–80° east of north) of this anisotropy are very similar to the results obtained in the Pacific Ocean off California. We tentatively conclude that this anisotropy is present as a consequence of the subduction of oceanic lithosphere beneath the western United States.

## 1 Introduction

There is now little doubt that the upper mantle is anisotropic, at least in part. Laboratory studies indicate that anisotropy in candidate upper mantle rocks is the rule rather than the exception (e.g. Peselnick, Nicolas & Stevenson 1974; Peselnick, Lockwood & Stewart 1977) and there is a considerable amount of seismic evidence of *in situ* anisotropy beneath continents and oceans (Bamford & Crampin 1977). However, while there is a consensus that the anisotropy probably results from the preferred orientation of olivine crystals, the presently available results do not discriminate between the various tectonic processes which might induce such preferred orientations.

There are at least three possible mechanisms, each of which would lead to different configurations of anisotropy throughout the lithosphere. Crampin (1977a) has summarized the following two possibilities: if, for example, there exists a deformation process which can induce preferred orientations in 'cold' lithosphere, the alignments would eventually be modified to conform with the present long-term stress pattern; one would then expect a uniform anisotropy, regardless of depth within the lithosphere. On the other hand, it could be that the alignments are induced at the lithosphere–asthenosphere boundary and are then

'frozen in' as the lithosphere cools: the anisotropy might then vary with depth corresponding to the historical variation in stress directions at the base of the thickening lithosphere. In both of these mechanisms, one would expect the anisotropy in any given depth range to be relatively consistent over large areas, probably over complete lithospheric plates.

We suggest, in contrast to these two mechanisms, that it is possible that preferred orientations might be induced during relatively localized tectonic events, for example when the Moho is re-established by differentiation in a region that is undergoing strong horizontal motion: the anisotropy might then be confined to a restricted depth range (or decrease with depth) with directions intimately related to the contemporary tectonics.

Thus a prime requirement is for studies of the presence, absence and variation of anisotropy at different depths beneath oceans and continents. One useful contribution would be to add to the studies of sub-Moho anisotropy based on $P_n$ refraction studies, so far undertaken beneath oceans (Raitt *et al.* 1971) and continents (Bamford 1977), by utilizing existing seismic refraction data.

This approach has been used by Bibee & Shor (1976) for further studies of crustal and upper mantle anisotropy in the Pacific Ocean. Here we apply the methods of Bamford (1977) to $P_n$ studies in *three* continental areas, namely northern Britain and the eastern and western United States.

## 2 The measurement of refractor velocity anisotropy

### 2.1 SUITABLE OBSERVATIONS

Several authors (Raitt *et al.* 1969; Morris, Raitt & Shor 1969; Bamford 1976, 1977) have shown that, given a suitable distribution of good quality time–distance data, the presence of refractor velocity anisotropy can be reliably recognized and its magnitude, direction and form adequately measured. The analysis is a two-stage process in which the time-term method is first applied to separate the effects of velocity variation from those of refractor topography and structure above the refractor: a resultant velocity is then computed for each observation and plotted as a function of azimuth in a 'velocity scattergram' (Bamford 1977). Further elaboration of the basic approach is not required here but it is appropriate to review the main observational requirements for anisotropy studies.

The prime requirement is for the reliable recognition and accurate timing of the refracted phase of interest. Both aims are best achieved by using reduced travel-time record sections from closely spaced observations on profiles: $P_n$, for example, can then be clearly separated from other first arrivals which travel through the crust or are returned from sub-Moho horizons in the lower lithosphere.

Secondly, it is clear that a minimum requirement for the detection and measurement of velocity anisotropy is that observations be made in several directions through the same piece of rock. However, for the real Earth the criteria become more severe if one is to detect and measure velocity anisotropy amidst the other complexities, such as lateral heterogeneity, which can have a similar effect on travel times. In principle, the presence of anisotropy can be recognized by using the $F$ ratio to compare the quality of fit to the data of a model which allows for anisotropy with that for a model which does not: the $F$ ratio is the ratio of the variances (sum of squared residuals/degrees of freedom) of the unmodified and modified solutions (Davies 1961). Statistical tables are then consulted to see if the derived $F$ ratio represents a significant improvement at a suitable confidence level, usually 90 or 95 per cent. This assumes that any inadequacy in the unmodified solution, for example, velocity anisotropy not allowed for, will swell the residual distribution. Unfortunately, one of the problems of time-term analysis (Bamford 1971), in which many delay times are determined

in addition to a few velocity parameters, is that an inadequate specification of the form of the refractor velocity may simply be reflected in systematically inaccurate delay times: the residual population may only be marginally swelled, if at all. This problem may be overcome by using an optimum observation scheme in which each site for which a delay time is determined has observations in as many different directions as possible.

Thirdly, the accurate determination of the parameters of the velocity anisotropy is dependent upon having a relatively even distribution of observations with respect to azimuth: gaps in the azimuth distribution should be avoided (Bamford 1977).

All of the above requirements are difficult to achieve in the composite, and typically rather heterogeneous, observation schemes with which this study is concerned. In fact, analysis is only made possible by using the MOZAIC time-term method of Bamford (1976). This method is based on the premise that within the region of study there exist small areas over which the delay time to a particular refractor is constant and that the distribution of such areas may be intelligently guessed at using ancillary information such as gravity or geological maps. Whilst it is then possible to use the resulting MOZAIC network to carry out a time-term analysis of otherwise unsuitable data, the suitability of any one MOZAIC for anisotropy studies is rarely immediately obvious. Thus, model studies have been carried out for all MOZAICs used here so as to obtain a better understanding of their basic capabilities for detecting and measuring refractor velocity anisotropy.

## 2.2 VELOCITY ANISOTROPY

A weak anisotropy of refractor velocity can be expressed by (Backus 1965; Crampin 1977b)

$$V_P^2 = V_0^2 + B\cos 2\phi + C\sin 2\phi + E\cos 4\phi + F\sin 4\phi \tag{1}$$

where $\phi$ is the azimuth measured clockwise from north. The coefficients $V_0^2$, $B$, $C$, $E$ and $F$ can be written as a function of the density and linear arrangements of six elastic constants rotated so that $x_1$ is the $\phi = 0$ direction and $x_3$ is normal to the surface. The velocity anisotropy encountered in the uppermost mantle is typically weak (< 10 per cent).

This general form is that actually used in studies of refractor velocity anisotropy, both in the time-term analyses and in fits to the velocity–azimuth data displayed in the scattergrams. However, if a vertical plane of symmetry exists then angles $\theta$ can be measured from a direction of sagittal symmetry and

$$V_P^2 = V_0'^2 + B'\cos 2\theta + C'\cos 4\theta \tag{2}$$

where the density and linear arrangements of four elastic constants determine $V_0'^2$, $B'$ and $C'$. If one then returns to measuring angles ($\phi$) from north, then $\theta = \phi - \phi_0$ where $\phi_0$ is the symmetry direction, and hence (Crampin & Bamford 1977)

$$\begin{aligned} V_P^2 = {} & V_0'^2 + (B'\cos 2\phi_0)\cos 2\phi + (B'\sin 2\phi_0)\sin 2\phi \\ & + (C'\cos 4\phi_0)\cos 4\phi + (C'\sin 4\phi_0)\sin 4\phi \end{aligned} \tag{3}$$

which is of the same form as (1).

It is important to note that only the relative amplitude of the cos $4\theta$ term in (2) provides any discriminatory measure to distinguish between different anisotropic structures (Crampin & Bamford 1977). However $C'$ is typically much smaller than $B'$ ($C'$ is one-sixth of $B'$ for (001)-cut olivine, Crampin & Bamford 1977) and is difficult to determine in the face of normal measurement errors.

For the model studies, a velocity anisotropy of form (2) has been assumed with $B'$: $C' = 6:1$; model velocities have been derived from

$$V_P^2 = (8.1)^2 + Q \cos 2(\phi - \phi_0) + Q/6 \cos 4(\phi - \phi_0) \quad (4)$$

with $Q = 4.0$, 2.0 and 1.0 (i.e. about 6, 3 and 1.5 per cent anisotropy respectively) and symmetry directions ($\phi_0$) of 0, 20, 40, 60 and 80° east of north. For each of the three observation schemes used here, exact model travel times were generated assuming this velocity variation together with the crustal structure/Moho topography that resulted from preliminary interpretations of the real data: these model travel times were then perturbed with a randomly generated 'measurement error', the standard deviation of which was that of the real data.

### 2.3 LATERAL VARIATIONS IN REFRACTOR VELOCITY

A common criticism of refractor velocity anisotropy results is that they are artifacts which arise because of a biased sampling of a laterally varying refractor velocity by an inadequate observation scheme: for example, observations subparallel to north–south lie predominantly in a region of high velocity, observations subparallel to east–west in a region of low velocity. In a well-designed experiment, it is possible to test this analytically by allowing the refractor velocity within the time-term solutions to vary as a polynomial function of position and conclude that a true anisotropy is present: see, for example, the oceanic $P_n$ studies of Raitt *et al.* (1969) and Morris *et al.* (1969). This is much more difficult in a continental study that uses a composite and therefore possibly ill-conditioned observation scheme although Bamford (1973, 1977) was able to do it for his $P_n$ study in Western Germany.

In practice, however, it is possible that the specification of refractor velocity variations as a polynomial function of position may not be an appropriate description of the variations that actually occur in the real Earth. This may be especially true in tectonically complex continental areas and the approach used in the present study was, where appropriate, to plot the individual velocity values, which for anisotropy studies are plotted in a scattergram as a function of azimuth, as a function of position. Simple contouring was then attempted to identify possible lateral velocity variations.

## 3 Eastern United States

### 3.1 THE DATA

This study concentrates on the area between the Appalachians and the Atlantic continental margin of the United States. Data are available from two experiments. First, the East Coast Onshore–Offshore Experiment (ECOOE) with a large number of shots offshore and many stations and a few shots onshore (Fig. 1): secondly, a land-based experiment carried out by the US Geological Survey for the calibration of their Cumberland Plateau Observatory (Fig. 1; henceforth CPOE). The available data are in the form of time–distance information, mostly for first arrivals, in Hales *et al.* (1968) for ECOOE and Borcherdt & Roller (1966) for CPOE. Thus neither record sections nor original seismograms were used in this study although the few ECOOE record sections published by Lewis & Meyer (1977) were used as a guide to phase correlations.

The preliminary data analysis consisted of plotting time–distance graphs (in ECOOE, for each station; in CPOE, for each shot) and using them to identify the basic pattern of travel-time branches. Additional published information was used where possible, for example the arrival quality/amplitude information given by Hales *et al.*: in this respect it was interesting to note a tendency for supposed $P_n$ arrivals to be somewhat better observed at longer distances, say beyond about 300 km. In this way broad time–distance envelopes could be defined corresponding to a general scheme of arrivals: Fig. 2 shows the slightly

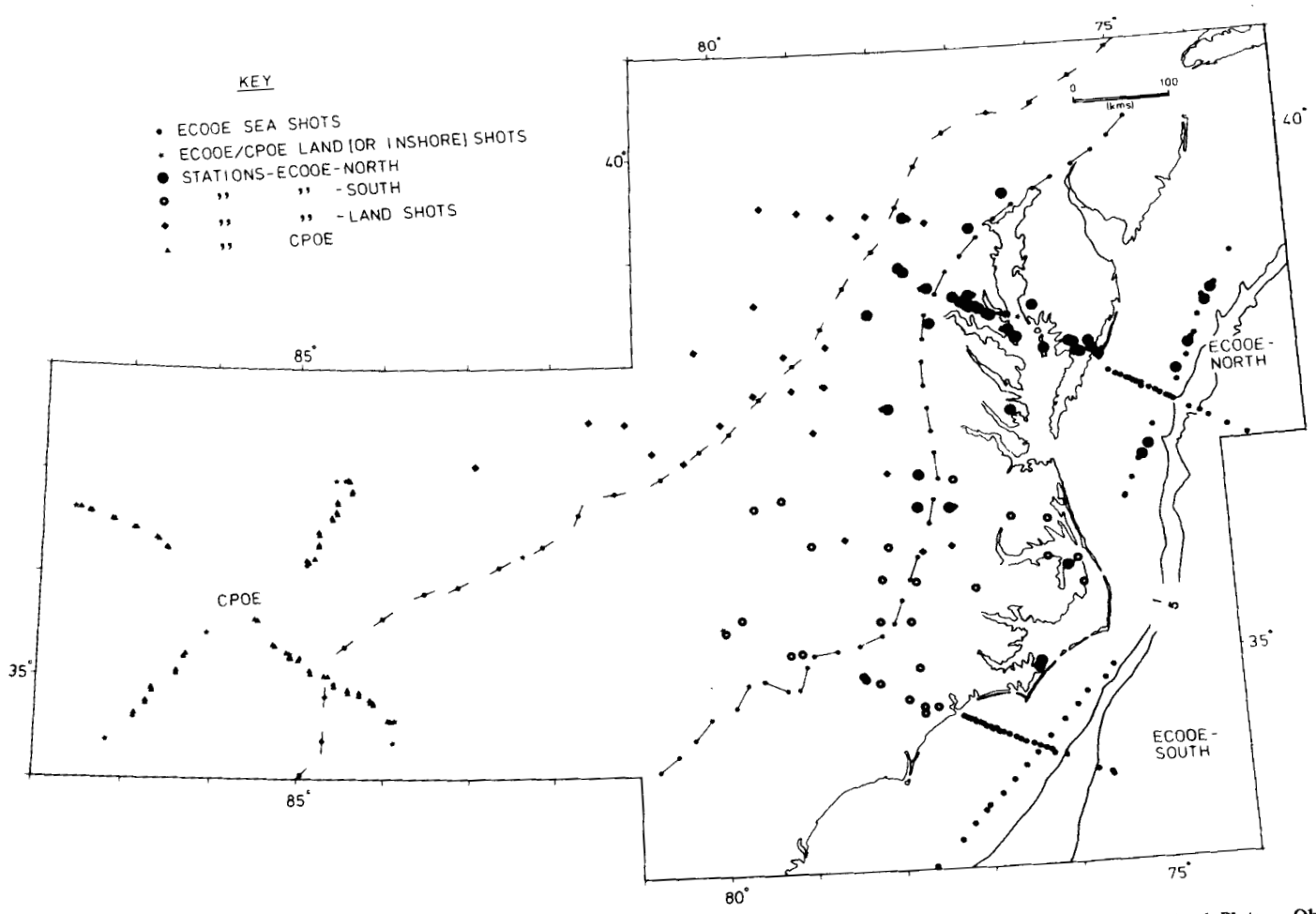


**Figure 1.** Location of shots and stations, eastern United States. ECOOE: East Coast Onshore–Offshore Experiment. CPOE: Cumberland Plateau Observatory Experiment. —◆—: Western edge of Appalachian core. ●—●: Edge of coastal plain. Bathymetric contours are in thousands of feet.

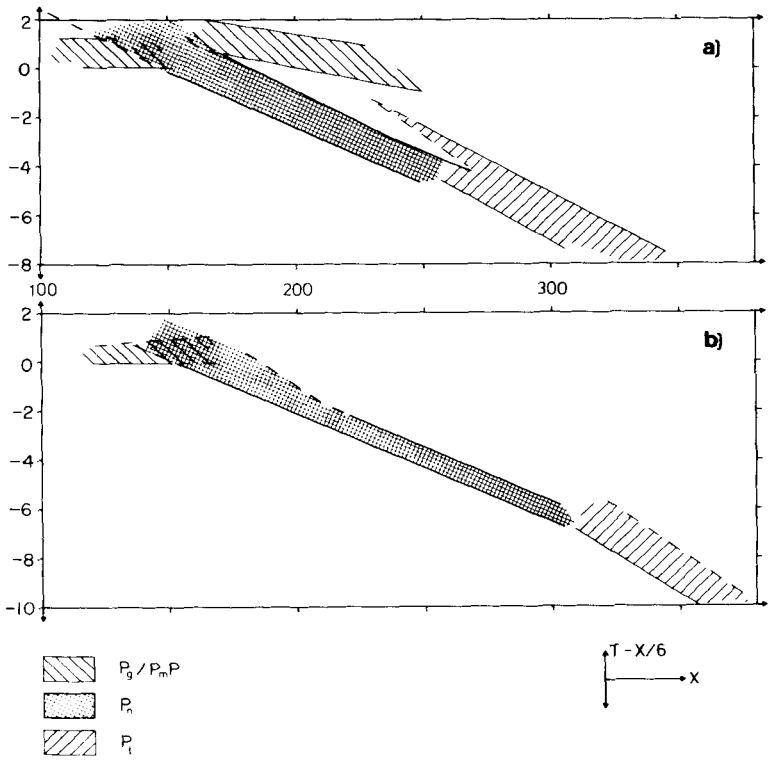


**Figure 2.** Reduced time–distance envelopes for various phases, ECOOE. (a) Northern and (b) southern sea-shots. $P_g/P_MP$ are crustal arrivals, $P_l$ is an arrival travelling through the lower lithosphere.

different schemes for the northern and the southern ECOOE sea-shots. Time–distance data were accepted as $P_n$ only if they lay within the appropriate time–distance envelope. Some 600 time–distance observations (weighted according to quality) were so accepted, mostly restricted to the distance range 150–300 km and distributed amongst the shots and stations shown in Fig. 1. ECOOE shots from the continental slope and ocean basin were mostly not included, and most of the ECOOE landshots appeared to give relatively unreliable travel times (see also James, Smith & Steinhart 1968).

The resulting data set is rather restricted in comparison to that used in the crustal study of the Middle Atlantic States by James *et al.* and has several serious disadvantages. First, it is effectively derived from three separate experiments, the northern ECOOE, the southern ECOOE and the CPOE, linked together only by a very few common or adjacent stations and shotpoints. Secondly, both the northern and the southern ECOOE sections are almost unreversed, with stations mainly to the west and shots to the east, and in fact the calculation of a true velocity is critically dependent upon the inclusion of the poor quality land-shot data and upon the few sites in the middle of the network that can be arranged (i.e. in a MOZAIC) so as to be connected to both the northern and the southern ECOOE shots. Thirdly, the azimuthal distribution of observations, Fig. 3, is strongly biased towards the north-west–south-east direction of the main ECOOE shot-station configuration (Fig. 1).

Thus, in spite of the fact that many of the ECOOE stations observed shots at various azimuths and vice versa, the composite data set must be regarded as ill-conditioned for any MOZAIC analysis and as only marginally suitable for anisotropy studies. This assessment may be checked by considering the model studies, for one possible MOZAIC, summarized

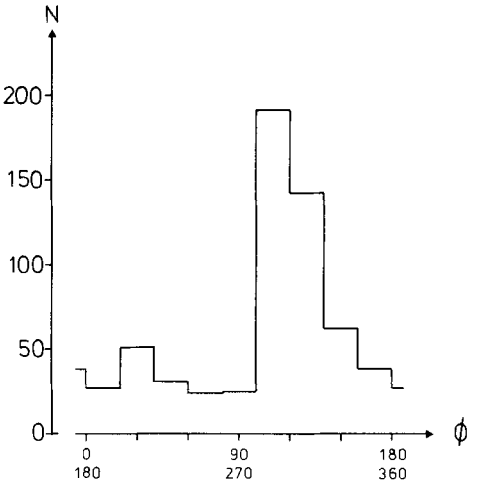


**Figure 3.** Azimuth distribution of available $P_n$ data, eastern United States, number of observations ($N$) versus azimuth ($\phi$).

in Table 1. The 'measurement errors' alone should result in a variance of about 0.039 $s^2$ and the critical $F$ ratio for significance at the 95 per cent level is 1.16: on this basis, a simple comparison of variances would certainly fail to detect any anisotropy of 3 per cent or less. On the other hand the computed anisotropy coefficients – especially $B$ and $C$, those for the $2\phi$ terms – remain reasonably accurate even down to the 1.5 per cent level. This suggests that the detection of velocity anisotropy with this network would be best achieved by analysis of the velocity scattergram.

### 3.2 RESULTS

Several MOZAIC studies, based on gravity, tectonic and basement maps of the eastern USA, have been attempted with this data set. Many were rather unsatisfactory due to the distribution and quality of the data but none of them gave any indication that velocity anisotropy was required by the data. As an example, MOZAIC 4A, based on basement/tectonic maps and using 430 observations based on 95 sites, gave the same variance (0.037 $s^2$) for both uniform and anisotropic velocity solutions: the resulting anisotropy coefficients (and of course the $F$ ratio) were not statistically significant at any meaningful confidence level (Table 1).

The final velocity scattergram (Fig. 4) shows no visible evidence of anisotropy, and a formal comparison of uniform velocity and anisotropic fits (equation (1)) through the corresponding velocity–azimuth data indicates no significant directional dependence ($F$ ratio = 1.003). Thus the hypothesis that the upper mantle is here *isotropic* (velocity approximately 8.2 km/s) is acceptable within the limits of observational error (which the mode studies and Fig. 4 place at about the 1 per cent anisotropy level or slightly higher).

## 4 Northern Britain

### 4.1 THE DATA

This study is based on several seismic experiments in and around northern Britain but in particular on the 1974 LISPB experiment. The high-quality LISPB record sections (Bamford *et al.* 1978) provide an opportunity for a reassessment or reinterpretation of data obtained

**Table 1.** Eastern United States: results.

(a) Model studies

| Model[1] $(Q/\phi_0)$ | Uniform velocity solution variance ($s^2$) | Variance ($s^2$) | $V_0$[3] | General anisotropy solutions: computed velocity coefficients[2] $B$ | $C$ | $E$ | $F$ | $F$ ratio |
|---|---|---|---|---|---|---|---|---|
| 4/0 | 0.048 | 0.039 | 8.16 | 3.72 (4.00) | −0.24 (0.00) | 0.77 (0.67) | 0.05 (0.00) | 1.21 |
| 4/20 | 0.051 | 0.039 | 8.15 | 2.78 (3.06) | 2.30 (2.57) | 0.27 (0.12) | 0.67 (0.66) | 1.29 |
| 4/40 | 0.048 | 0.039 | 8.15 | 0.42 (0.69) | 3.66 (3.93) | −0.42 (−0.63) | 0.28 (0.23) | 1.23 |
| 4/60 | 0.045 | 0.039 | 8.15 | −2.24 (−2.00) | 3.19 (3.46) | −0.14 (−0.33) | −0.47 (−0.58) | 1.15 |
| 4/80 | 0.047 | 0.039 | 8.15 | −3.98 (−3.76) | 1.09 (1.37) | 0.65 (0.51) | −0.30 (−0.43) | 1.20 |
| 2/0 | 0.041 | 0.039 | 8.16 | 1.74 (2.00) | −0.24 (0.00) | 0.48 (0.33) | 0.07 (0.00) | 1.04 |
| 2/20 | 0.041 | 0.039 | 8.16 | 1.27 (1.53) | 1.03 (1.29) | 0.22 (0.06) | 0.38 (0.33) | 1.06 |
| 2/40 | 0.041 | 0.039 | 8.16 | 0.09 (0.35) | 1.71 (1.97) | −0.14 (−0.31) | 0.18 (0.11) | 1.04 |
| 2/60 | 0.040 | 0.039 | 8.16 | −1.26 (−1.00) | 1.48 (1.73) | 0.01 (−0.17) | −0.21 (−0.29) | 1.03 |
| 2/80 | 0.041 | 0.039 | 8.16 | −2.14 (−1.88) | 0.43 (0.68) | 0.41 (0.26) | −0.13 (−0.21) | 1.05 |
| 1/0 | 0.039 | 0.039 | 8.16 | 0.74 (1.00) | −0.25 (0.00) | 0.33 (0.17) | 0.07 (0.00) | 1.00 |
| 1/20 | 0.039 | 0.039 | 8.16 | 0.50 (0.77) | 0.39 (0.64) | 0.20 (0.03) | 0.23 (0.16) | 1.00 |
| 1/40 | 0.039 | 0.039 | 8.16 | −0.09 (0.17) | 0.74 (0.98) | 0.01 (−0.16) | 0.13 (0.06) | 1.00 |
| 1/60 | 0.039 | 0.039 | 8.16 | −0.76 (−0.50) | 0.62 (0.87) | 0.09 (−0.08) | −0.07 (−0.14) | 1.00 |
| 1/80 | 0.040 | 0.039 | 8.16 | −1.19 (−0.94) | 0.10 (0.34) | 0.29 (0.13) | −0.03 (−0.11) | 1.01 |

(b) Real data

| | | | | | | | | |
|---|---|---|---|---|---|---|---|---|
| | 0.037 | 0.037 | 8.23 | −0.60 | −0.05 | 0.22 | 0.31 | 1.00 |
| Standard errors[4] in computed velocity coefficients: | | | | ±0.05 | ±0.49 | ±0.51 | ±0.36 | ±0.27 |

(1) Parameters $(Q/\phi_0)$ used in equation (4).
(2) These coefficients correspond to those in equation (1): for the model studies, the values in brackets are the theoretical values of the coefficients.
(3) Model value 8.1 km/s.
(4) These errors apply to solutions for both the model and the real data.

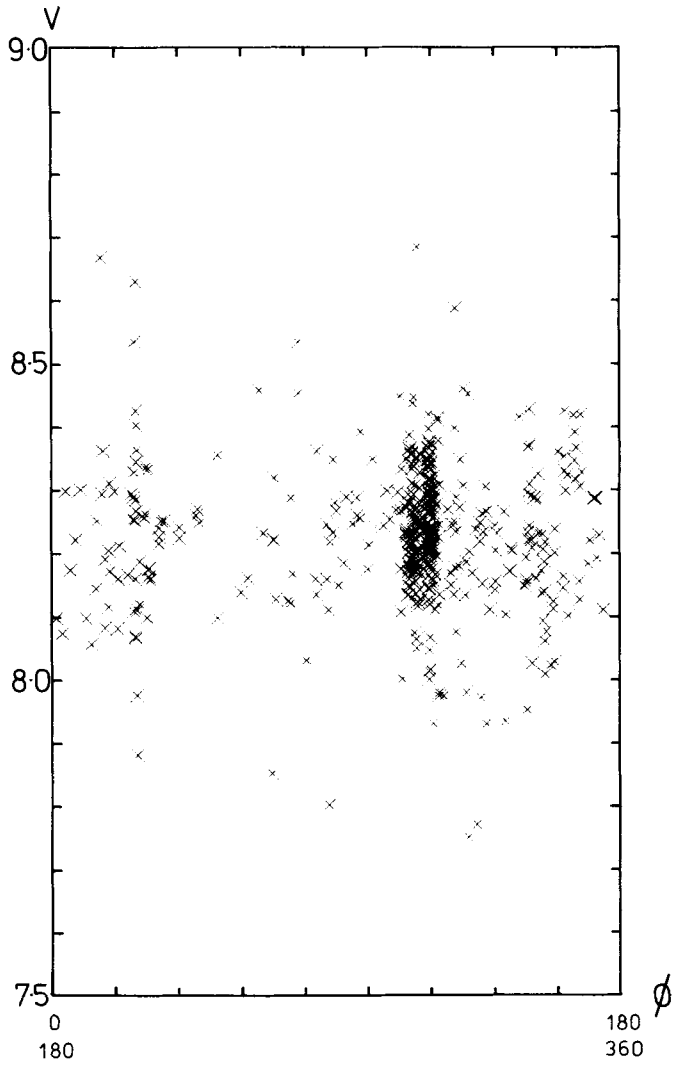


**Figure 4.** Final velocity scattergram, eastern United States, velocity ($V$) versus azimuth ($\phi$).

in earlier experiments, with special emphasis on the correct identification of the $P_n$ phase over a limited range of observation distances only.

The earlier experiments include the North Atlantic Seismic Project (NASP, Smith & Bott 1975), the Norway–Scotland $P_n$ Project (Sornes 1968), the ten-ton shot programme (Jacob & Willmore 1975) and the various explosions fired around Scotland known collectively as the Scottish Offshore Seismic Program (SOSP, Jacob 1975). Recordings are available from mobile stations and from the LOWNET seismic array in central Scotland. Time–distance data, in some cases like NASP consisted of published values (Smith 1975) or, for all shots recorded on LOWNET, were derived from replayed and repicked seismograms. The signal/noise ratio of the seismograms was sometimes well below that of LISPB, in particular for the SOSP–LOWNET recordings, and the observations were weighted according to their quality relative to LISPB. All these data have been assessed using the LISPB-based time–

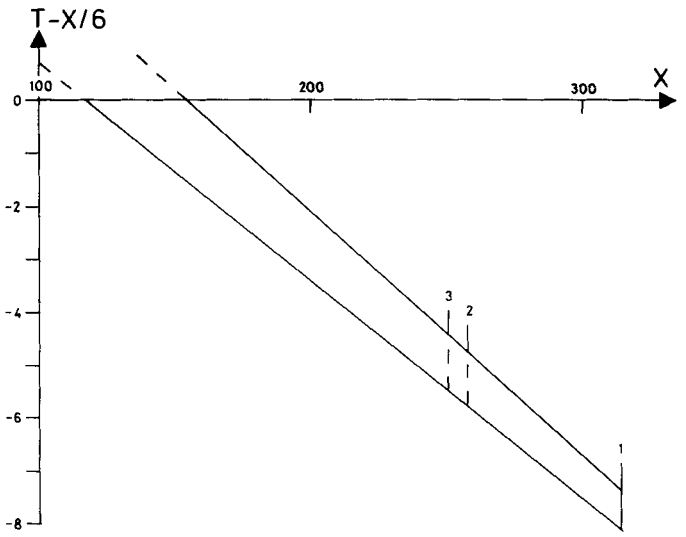


**Figure 5.** $P_n$ reduced time–distance envelope, northern Britain. Maximum observation distances: (1) LISPB, (2) NASP, (3) SOSP, Norway–Scotland $P_n$, ten-ton shots.

distance envelope of Fig. 5. An arrival was accepted as $P_n$ only if its time–distance value lay within this envelope: over 430 observations, derived from the shots and stations shown in Fig. 6, were so accepted.

The geographic distribution of shots and stations (Fig. 6) and the azimuthal distribution of observations (Fig. 7) are not ideal. The bulk of observations are concentrated close to either north–south (LISPB and NASP) or north-east–south-west (NASP). Furthermore many of the east–west observations are obtained from SOSP–LOWNET connections: these are considered less reliable than, and are somewhat removed geographically from, the rest of the observations which lie mainly within a large triangle to the north and east of Scotland (Fig. 6). On the other hand, many of the shots, especially those in NASP, are observed in several different directions, some of the recording stations are common between the various experiments, and the design of suitable MOSAICs was not found to be critically dependent upon the inclusion of certain observations.

The capabilities of this network can be further assessed by considering the model study results summarized in Table 2. The 'measurement error' alone should lead to a variance of about 0.034 $s^2$ and the critical $F$ ratio for significance at the 95 per cent confidence level is approximately 1.16: on this basis, anisotropy at the 3 per cent level would be barely detectable with a simple comparison of variances. In contrast, $B$ and $C$ – the velocity coefficients of the $2\phi$ terms – remain accurate down to the lowest level considered (1.5 per cent): this indicates that a velocity scattergram for this network might give a reliable indication of the presence of anisotropy down to at least this level, possibly rather less.

### 4.2 RESULTS

From the foregoing discussion, it would seem that this data set offers a reasonable opportunity to detect any significant anisotropy present, and in practice it was found that all the MOZAICs studied, based primarily on geological or tectonic maps of northern Britain, were satisfactory from the point of giving stable solutions etc. However, none of them gave

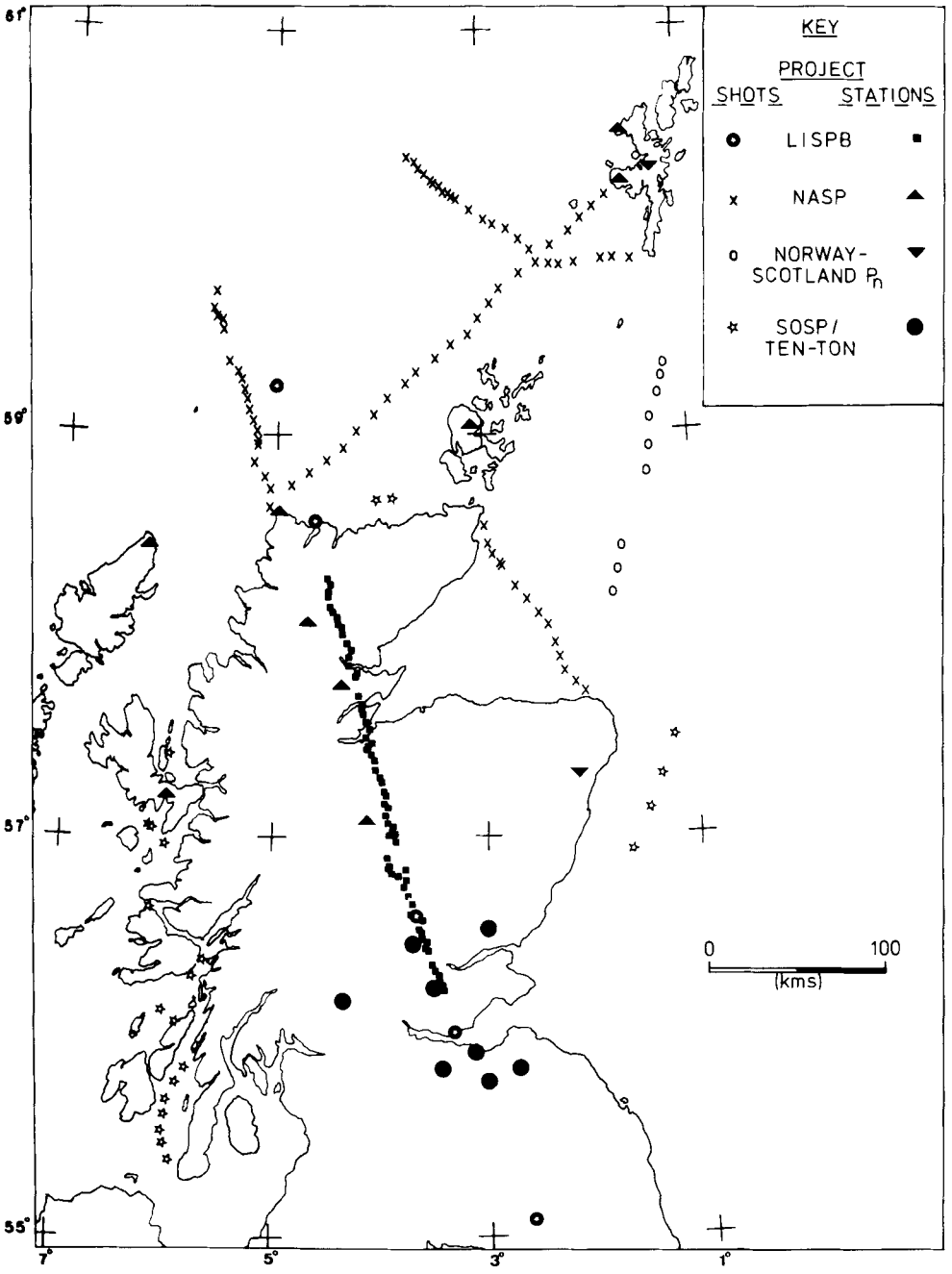


**Figure 6.** Distribution of shots and stations, northern Britain.

any indication that velocity anisotropy was required by the data. As an example, a typical MOZAIC using 427 observations based on 87 sites gave an $F$ ratio of 1.02 (variances ~ 0.034–0.035 $s^2$) for uniform and anisotropic velocity solutions. Neither this $F$ ratio nor the resulting anisotropy coefficients were significant at any meaningful confidence level (Table 2).

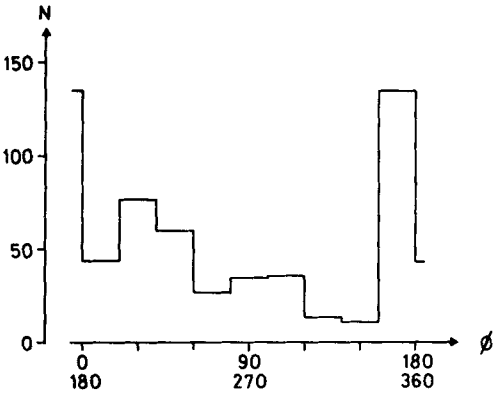


**Figure 7.** Azimuthal distribution of observations, northern Britain, number of observations ($N$) versus azimuth ($\phi$).

The final velocity scattergram (Fig. 8) shows no visible evidence of anisotropy, and a formal comparison of uniform velocity and anisotropic fits (equation (1)) through the corresponding velocity–azimuth data indicates no significant directional dependence ($F$ ratio = 1.001). Thus the hypothesis that the upper mantle is here *isotropic* (velocity approximately 8.0 km/s) is acceptable within the limits of observational error (which the model studies and Fig. 8 place at about the 1 per cent anisotropy level or slightly less).

## 5 Western United States

### 5.1 THE DATA

Two sources of data were utilized in this study:

(1) Sixty-three seismic refraction profiles measured in the early 1960s by the United States Geological Survey, primarily in the California–Nevada region but also in Idaho, Wyoming and Arizona (Fig. 9). The shots were chemical explosions except for underground nuclear devices fired at the Nevada Test Site (NTS) and SHOAL. Most of the profiles are reversed and all were available in the form of reduced travel-time record sections compiled by Prodehl (1970a, b, 1978) – examples are shown in Fig. 10.

(2) The relatively large amount of time–distance data published for the California–Nevada region. Especially important were two profiles from NTS, one from the Pahute Mesa to San Francisco Bay (Carder, Qamar & McEvilly 1970) and another through Death Valley to Monterey Bay (Carder 1973) – Fig. 9. Additional time–distance data from special shots, quarry blasts and NTS as recorded on the USGS, Berkeley and CIT networks and at various temporary stations, were taken from Lehmann (1962), Mikumo (1965), Carder *et al.* (1970), Kind (1972), Carder (1973), Allen & Helmberger (1973), Wesson, Roller & Lee (1973), Kanamori & Fuis (1976) and Kanamori & Hadley (1975).

For the profiles, the availability of the record sections (e.g. Fig. 10) made the recognition and timing of $P_n$ straightforward even though this phase is generally of relatively low amplitude in this area. The resulting time–distance data are mainly restricted to observation distances of less than 300 km – at greater distances, stronger and slightly later arrivals seem

**Table 2.** Northern Britain: results.

(a) Model studies

| Model[1] ($Q/\phi_0$) | Uniform velocity solution variance ($s^2$) | Variance ($s^2$) | $V_0$[3] | General anisotropy solutions: computed velocity coefficients[2] $B$ | $C$ | $E$ | $F$ | $F$ ratio |
|---|---|---|---|---|---|---|---|---|
| 4/0 | 0.058 | 0.034 | 8.09 | 4.02 (4.00) | −0.32 (0.00) | 0.40 (0.67) | 0.22 (0.00) | 1.70 |
| 4/20 | 0.053 | 0.034 | 8.09 | 3.08 (3.06) | 2.25 (2.57) | −0.12 (0.12) | 0.80 (0.66) | 1.54 |
| 4/40 | 0.056 | 0.034 | 8.10 | 0.71 (0.69) | 3.64 (3.93) | −0.80 (−0.63) | 0.40 (0.23) | 1.64 |
| 4/60 | 0.058 | 0.034 | 8.10 | −2.02 (−2.00) | 3.15 (3.46) | −0.52 (−0.33) | −0.33 (−0.58) | 1.69 |
| 4/80 | 0.055 | 0.034 | 8.10 | −3.81 (−3.76) | 1.03 (1.37) | 0.24 (0.51) | −0.20 (−0.43) | 1.60 |
| 2/0 | 0.040 | 0.034 | 8.10 | 2.02 (2.00) | −0.33 (0.00) | 0.11 (0.33) | 0.21 (0.00) | 1.17 |
| 2/20 | 0.039 | 0.034 | 8.10 | 1.55 (1.53) | 0.97 (1.29) | −0.16 (0.06) | 0.52 (0.33) | 1.13 |
| 2/40 | 0.039 | 0.034 | 8.10 | 0.35 (0.35) | 1.66 (1.97) | −0.52 (−0.31) | 0.31 (0.11) | 1.15 |
| 2/60 | 0.040 | 0.034 | 8.10 | −1.02 (−1.00) | 1.41 (1.73) | −0.38 (−0.17) | −0.07 (−0.29) | 1.16 |
| 2/80 | 0.039 | 0.034 | 8.10 | −1.92 (−1.88) | 0.35 (0.68) | 0.03 (0.26) | −0.01 (0.21) | 1.14 |
| 1/0 | 0.035 | 0.034 | 8.10 | 1.01 (1.00) | −0.34 (0.00) | −0.05 (0.17) | 0.21 (0.00) | 1.04 |
| 1/20 | 0.035 | 0.034 | 8.10 | 0.78 (0.77) | 0.32 (0.64) | −0.20 (0.03) | 0.37 (0.16) | 1.02 |
| 1/40 | 0.035 | 0.034 | 8.10 | 0.17 (0.17) | 0.66 (0.98) | −0.37 (−0.16) | 0.27 (0.06) | 1.03 |
| 1/60 | 0.035 | 0.034 | 8.10 | −0.51 (−0.50) | 0.54 (0.87) | −0.30 (−0.08) | 0.06 (−0.14) | 1.03 |
| 1/80 | 0.035 | 0.034 | 8.10 | −0.97 (−0.94) | 0.01 (0.34) | −0.10 (0.13) | 0.10 (−0.11) | 1.03 |

(b) Real data

| | | | | | | | | |
|---|---|---|---|---|---|---|---|---|
| | 0.035 | 0.034 | 7.96 | 0.50 | −0.43 | −0.47 | 0.53 | 1.02 |
| Standard errors[4] in computed velocity coefficients: | | | | ±0.03 | ±0.30 | ±0.35 | ±0.25 | ±0.34 |

(1) Parameters ($Q/\phi_0$) used in equation (4).
(2) These coefficients correspond to those in equation (1): for the model studies the values in brackets are the theoretical values of the coefficients.
(3) Model value 8.1 km/s.
(4) These errors apply to solutions for both the model and the real data.

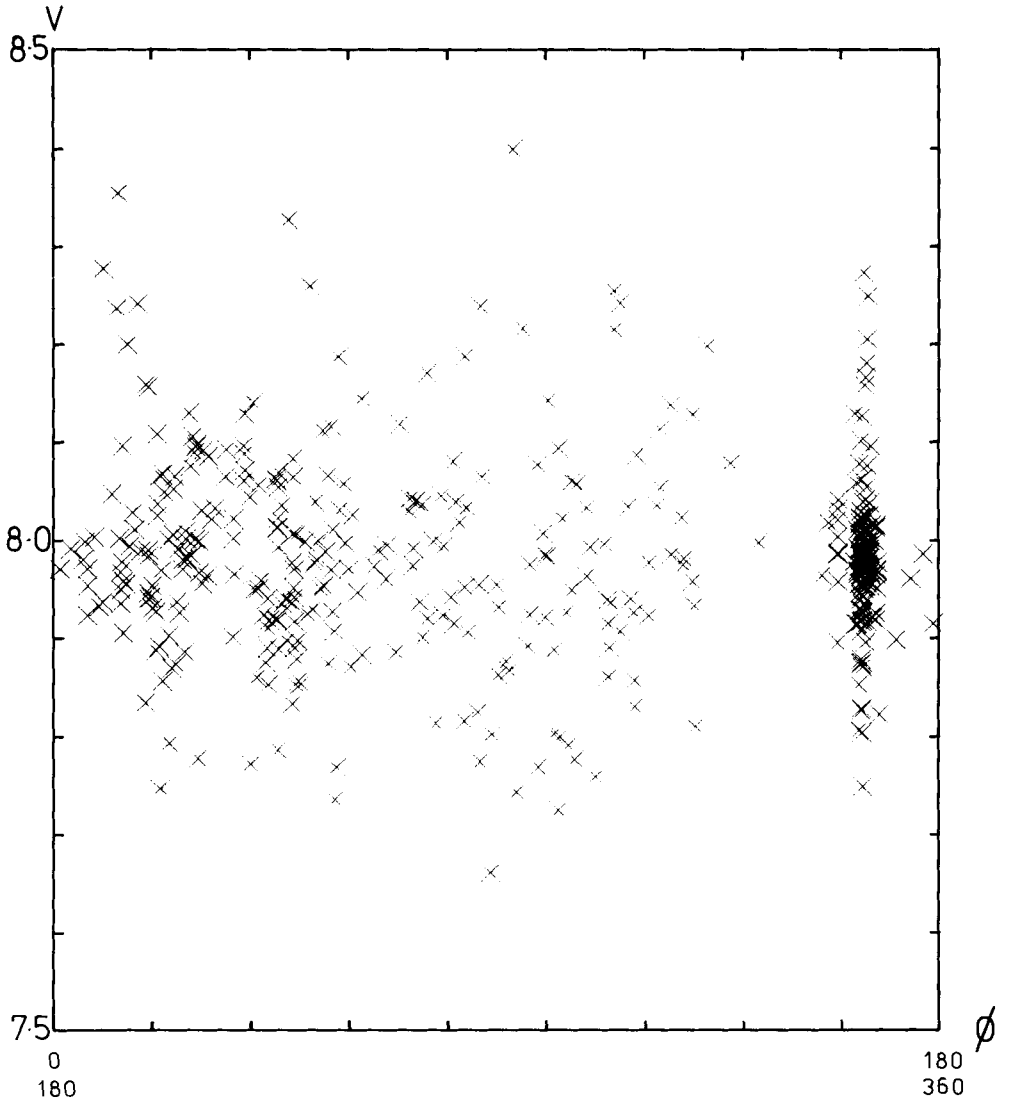


**Figure 8.** Final velocity scattergram, northern Britain, velocity ($V$) versus azimuth ($\phi$).

to correspond to energy that has been returned from the lower lithosphere, for example on the profile NTS–San Luis Obispo (Fig. 10(a)). The record sections also allowed an objective assessment of the published data that was only available in the form of time–distance values. For example, the profiles NTS–San Luis Obispo (Fig. 10(a)) and, to a lesser extent, NTS–Ludlow (Fig. 10(b)) could be used as a basis for the assessment of time–distance data for NTS as observed at stations in California – in fact the bulk of the data available. Fig. 11 shows a comparison between the NTS–San Luis Obispo travel-time branches and best straight lines fitted through the Pahute Mesa–San Francisco Bay and Death Valley–Monterey Bay time–distance data (Carder *et al.* 1970; Carder 1973) on the basis of which one may conclude that the published time–distance data indeed correspond to a true $P_n$ phase, even at observation distances beyond 300 km. Beyond about 400 km, however, there are indications of a faster, deeper penetrating phase. Fig. 11 was then used to assess other

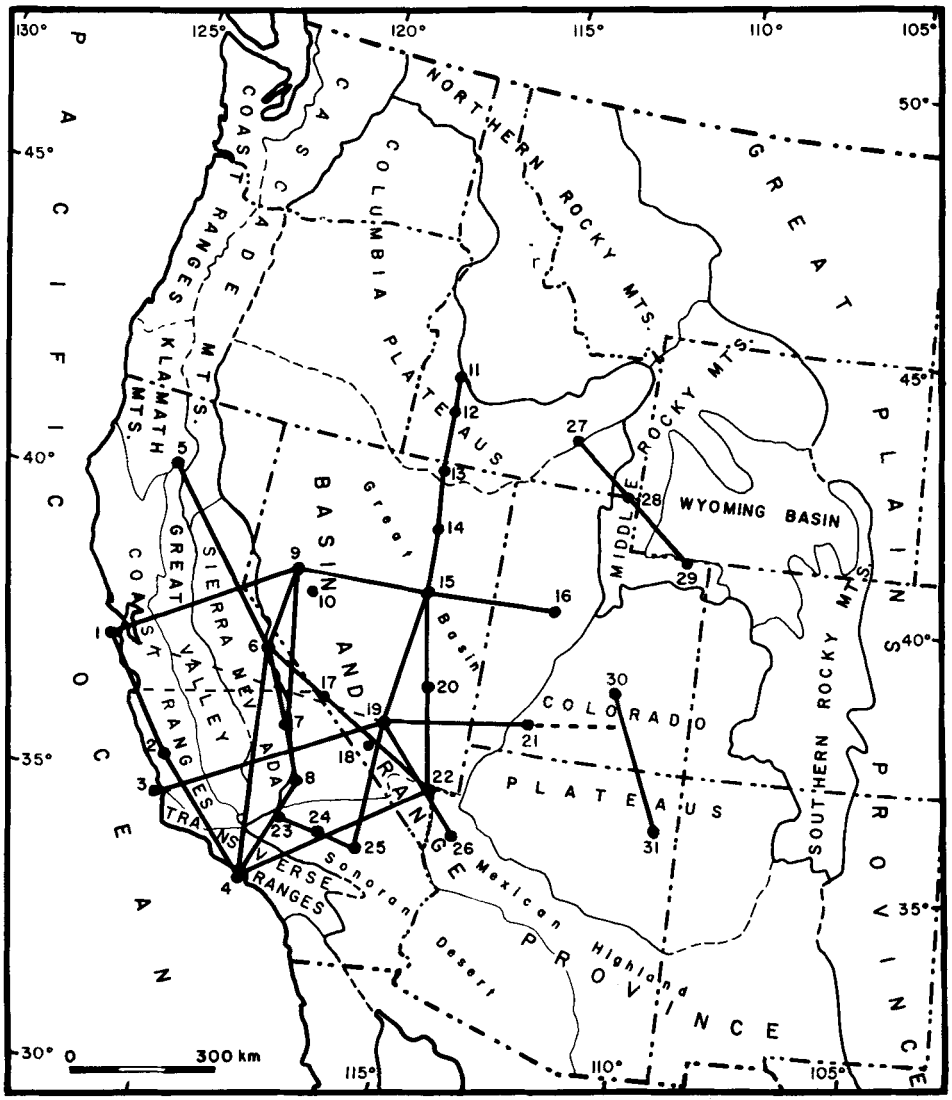


**Figure 9.** Physical divisions of the western United States and location of seismic profiles. Solid lines: United States Geological Survey profiles (after Prodehl 1970a, b). Broken lines: additional NTS profiles (Carder *et al.* 1970; Carder 1973). Shotpoints: 1 San Francisco, 2 Camp Roberts, 3 San Luis Obispo, 4 Santa Monica Bay, 5 Shasta Lake, 6 Mono Lake, 7 Independence, 8 China Lake, 9 Fallon, 10 Shoal, 11 Boise, 12 Strike Reservoir, 13 Mountain City, 14 Elko, 15 Eureka, 16 Delta, 17 Lida Junction, 18 Lathrop Wells, 19 Nevada Test Site, 20 Hiko, 21 Navajo Lake, 22 Lake Mead, 23 Mojave, 24 Barstow, 25 Ludlow, 26 Kingman, 27 American Falls Reservoir, 28 Bear Lake, 29 Flaming Gorge Reservoir, 30 Hanksville, 31 Chinle.

time–distance data for NTS as recorded at rather more scattered stations in California and Nevada as most of these observations in fact lie in the arc covered by the profiles NTS–Pahute Mesa–San Francisco Bay, NTS–Death Valley–Monterey Bay, NTS–San Luis Obispo and NTS–Ludlow (Fig. 9). Similarly, additional data in the Coast Ranges were assessed using record sections for profiles lying in the Coast Ranges (Fig. 9), and data in Southern California were assessed using record sections of profiles from Santa Monica Bay, Mojave

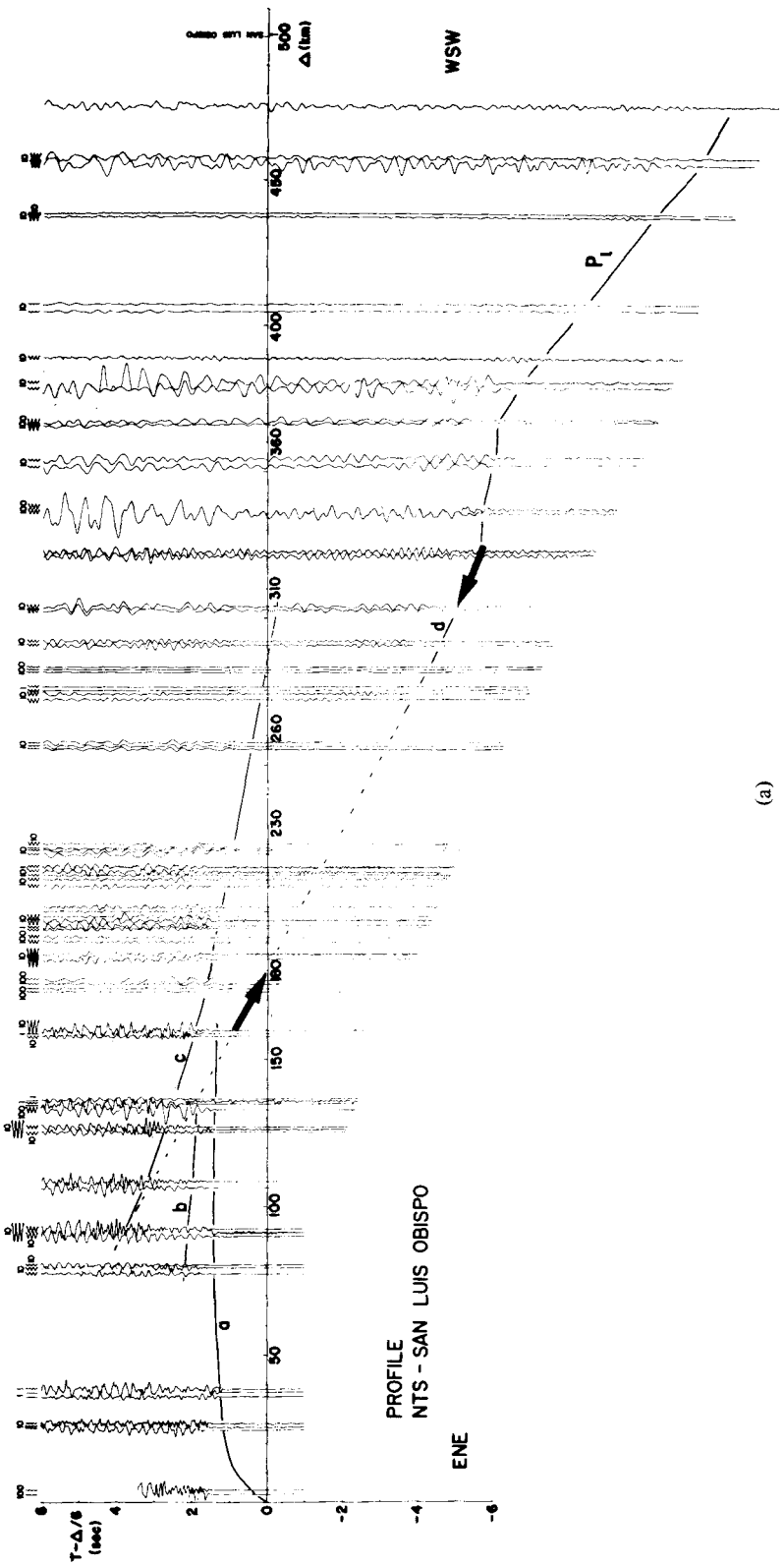


(a)

**Figure 10** Typical record sections: reduction velocity 6 km/s. (a) NTS–San Luis Obispo, (b) NTS–Ludlow, (c) Santa Monica Bay–China Lake. $P_n$ arrivals are indicated between the arrows on each section: $P_1$ is an arrival believed to have travelled through the lower lithosphere. The other correlations are those of Prodehl (1978).

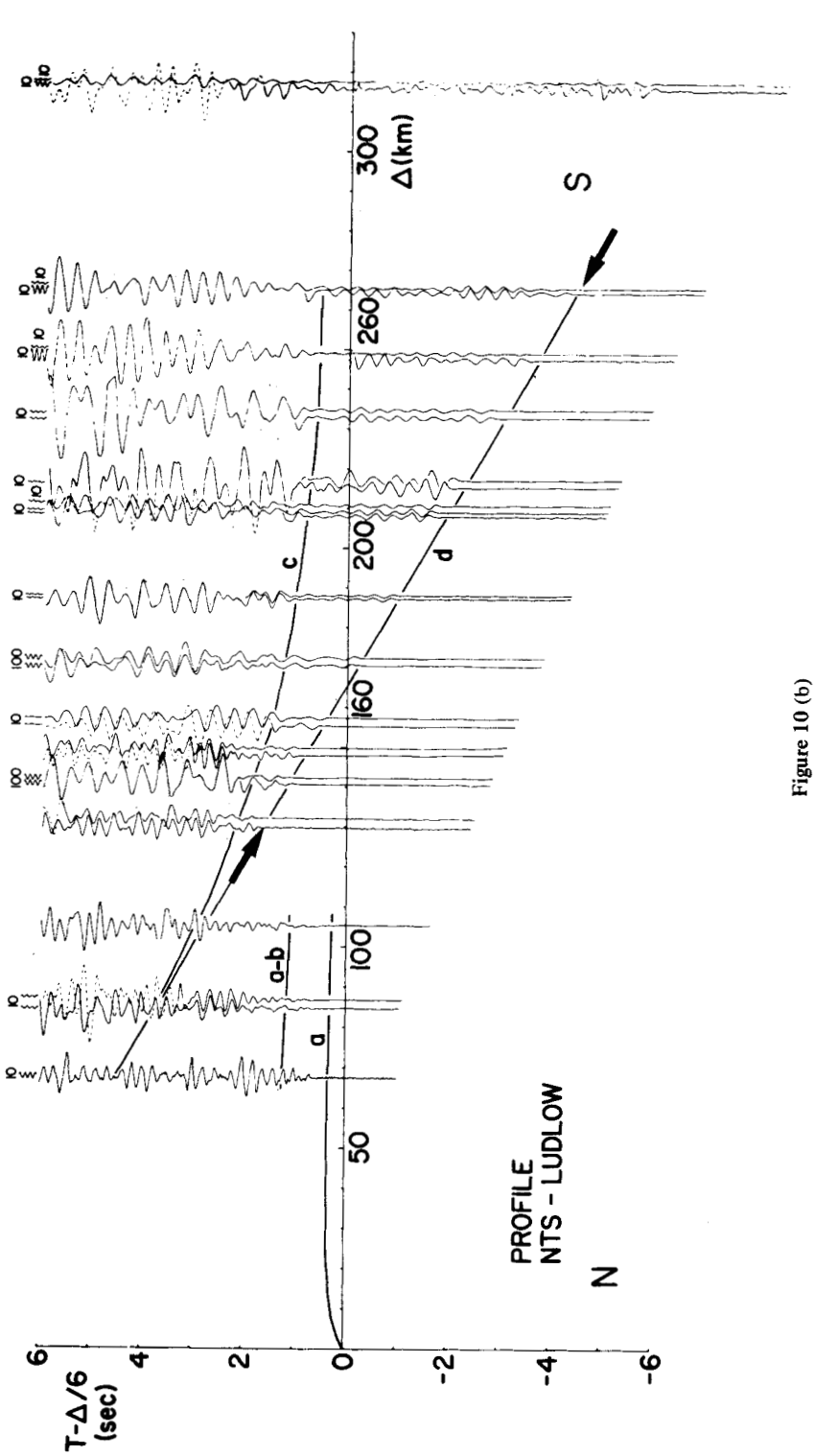


Figure 10 (b)

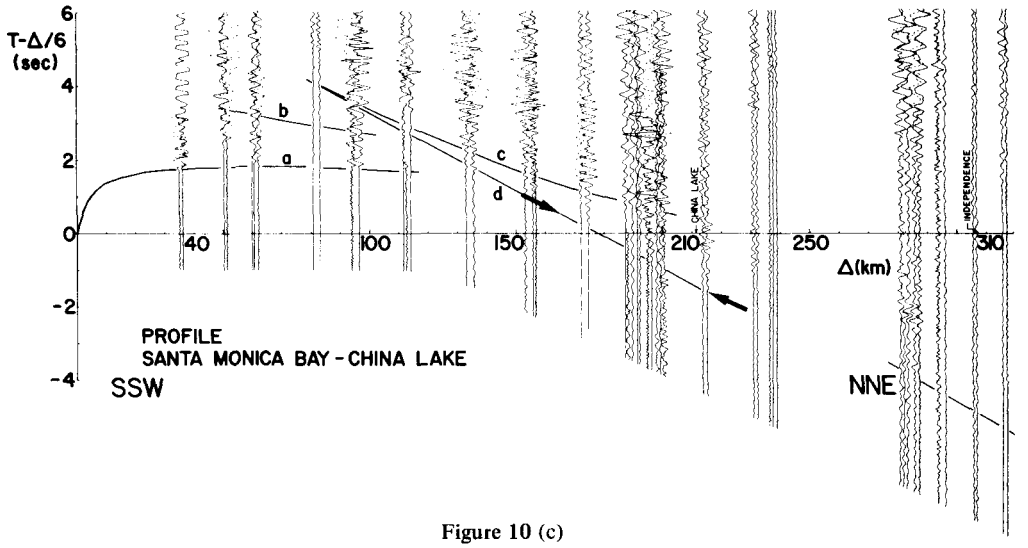


Figure 10 (c)

and China Lake (Figs 9 and 10(c)). The resulting data set contains 813 $P_n$ time–distance observations, weighted according to quality and with the distance distribution shown in Fig. 12(a). The majority of observations beyond 300 km distance are from published studies based on NTS; it may be that the relatively powerful sources available at NTS allowed the weak $P_n$ phase to be observed to somewhat greater distances than the chemical explosions normally used for the profiles. The azimuthal distribution of these observations is far from ideal (Fig. 12(b)) – in particular there is a pronounced gap for directions north-east–south-west. In practice, many of the observations were excluded from the analysis at an early stage for various reasons. For example, all observations from shotpoints 27–31 and all observations recorded to the north of shotpoint 15 from shotpoints 11–15 (Fig. 9) were excluded because they could not be connected with the other observations in any reasonable MOZAIC. Furthermore, profiles parallel to the coast in the Coast Ranges west of the San Andreas Fault (Fig. 9) were excluded after some preliminary analyses had confirmed that the Fault seems to separate rather differing structures with the crust 3–4 km thinner under,

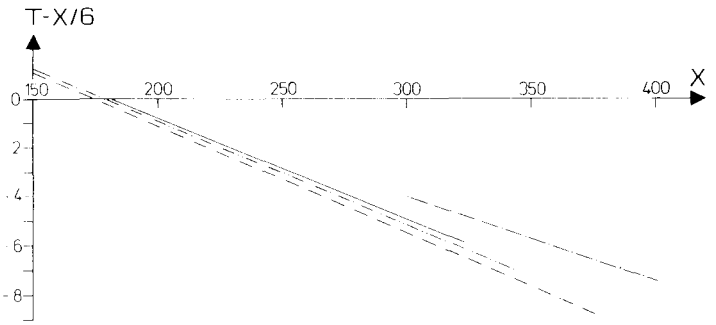


**Figure 11.** Reduced time–distance branches for:

NTS – San Luis Obispo (see Fig. 10(a)) $P_n$ ——— $P_1$ – . – . –

NTS – Pahute Mesa–San Francisco Bay $P_n$ – – – –

NTS – Death Valley–Monterey Bay $P_n$ – .. – .. –

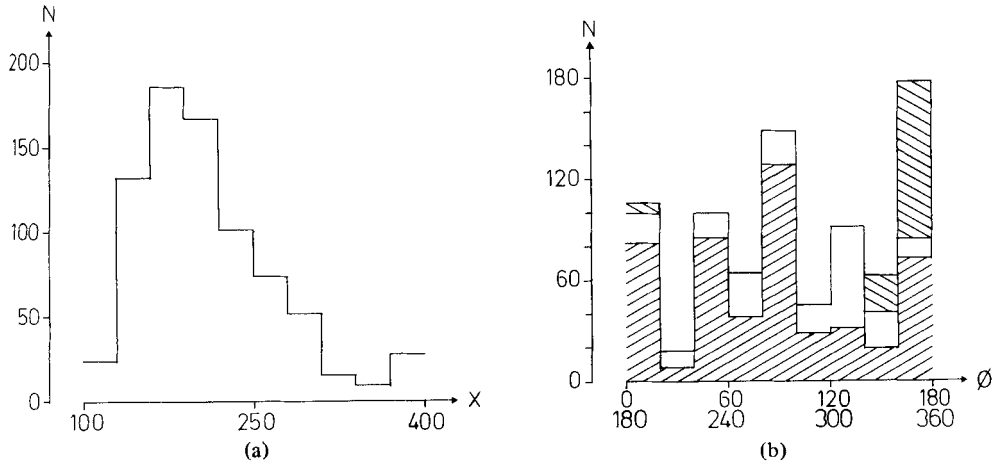


**Figure 12.** Distribution of available $P_n$ data, western United States: number of observations ($N$). (a) As a function of observation distance ($X$ in km). (b) As a function of azimuth ($\phi$). ▨ Data actually used in MOZAIC T.07. □ Extra data available in working data set. ▨ Additional data available in western United States but not included in working data set.

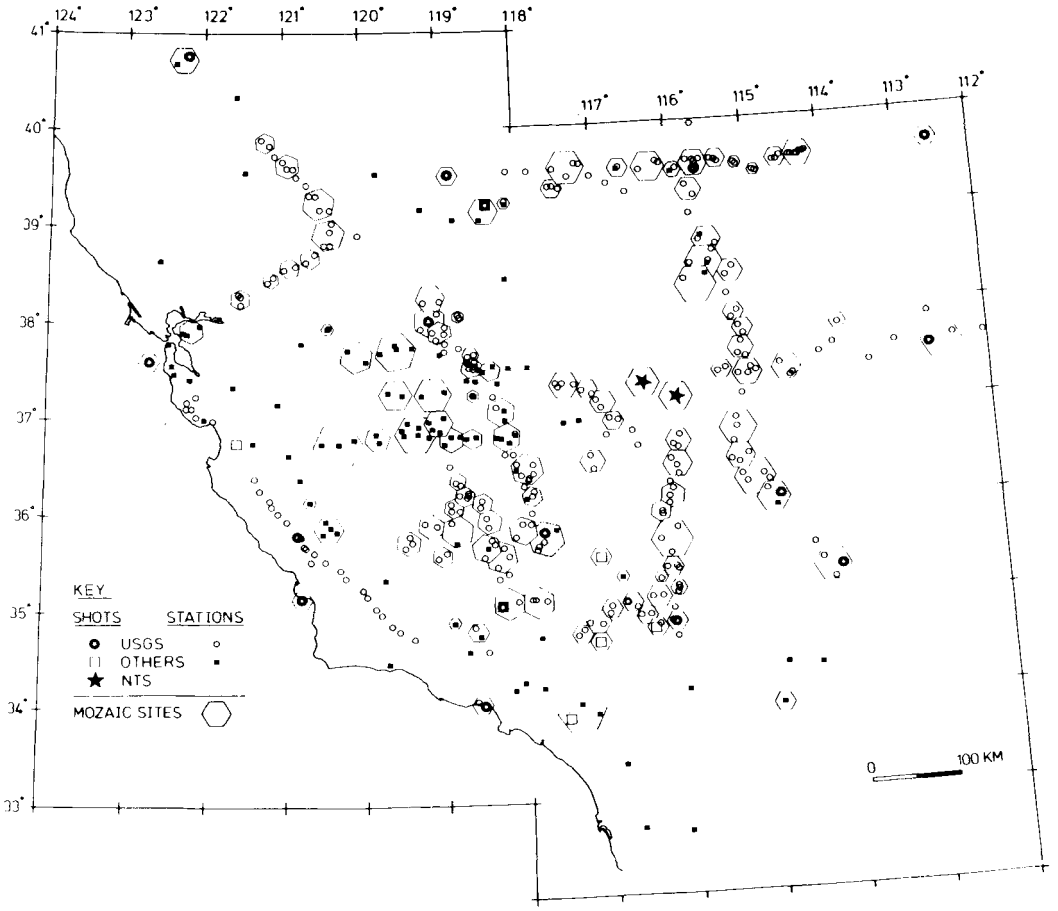


**Figure 13.** Distribution of shotpoints and stations for USGS profiles and other observations, western United States working data set, with typical MOZAIC (T.07).

Table 3. Western United States: summary of model studies for MOZAIC T.07.

| Model[1] ($Q/\phi_0$) | Uniform velocity solution variance ($s^2$) | Variance ($s^2$) | $V_0$[3] | General anisotropy solutions: computed velocity coefficients[2] $B$ | $C$ | $E$ | $F$ | $F$ ratio |
|---|---|---|---|---|---|---|---|---|
| 4/0 | 0.076 | 0.035 | 8.05 | 3.66 (4.00) | −0.14 (0.00) | 0.66 (0.67) | −0.32 (0.00) | 2.17 |
| 4/20 | 0.060 | 0.035 | 8.05 | 2.77 (2.57) | 2.36 (2.57) | 0.17 (0.12) | 0.25 (0.66) | 1.71 |
| 4/40 | 0.051 | 0.035 | 8.05 | 0.46 (0.69) | 3.67 (3.94) | −0.48 (−0.63) | −0.14 (0.23) | 1.46 |
| 4/60 | 0.069 | 0.035 | 8.05 | −2.17 (−2.00) | 3.20 (3.46) | −0.22 (−0.33) | −0.84 (−0.58) | 1.97 |
| 4/80 | 0.090 | 0.035 | 8.05 | −3.87 (−3.76) | 1.18 (1.37) | 0.52 (0.51) | −0.70 (−0.43) | 2.57 |
| 2/0 | 0.044 | 0.035 | 8.05 | 1.73 (2.00) | −0.14 (0.00) | 0.38 (0.33) | −0.33 (0.00) | 1.26 |
| 2/20 | 0.040 | 0.035 | 8.05 | 1.27 (1.53) | 1.11 (1.29) | 0.12 (0.06) | −0.03 (0.33) | 1.14 |
| 2/40 | 0.039 | 0.035 | 8.05 | 0.12 (0.35) | 1.77 (1.97) | −0.22 (0.31) | −0.23 (0.11) | 1.11 |
| 2/60 | 0.045 | 0.035 | 8.05 | −1.20 (−1.00) | 1.53 (1.73) | −0.08 (−0.17) | −0.60 (−0.29) | 1.29 |
| 2/80 | 0.051 | 0.035 | 8.05 | −2.05 (−1.88) | 0.52 (0.68) | 0.31 (0.26) | −0.52 (−0.21) | 1.46 |
| 1/0 | 0.037 | 0.035 | 8.05 | 0.75 (1.00) | −0.14 (0.00) | 0.23 (0.17) | −0.33 (0.00) | 1.06 |
| 1/20 | 0.036 | 0.035 | 8.05 | 0.53 (0.77) | 0.48 (0.64) | 0.10 (0.03) | −0.17 (0.16) | 1.03 |
| 1/40 | 0.036 | 0.035 | 8.05 | −0.05 (0.17) | 0.81 (0.98) | −0.08 (−0.16) | −0.26 (0.06) | 1.03 |
| 1/60 | 0.038 | 0.035 | 8.05 | −0.71 (−0.50) | 0.69 (0.87) | −0.01 (−0.08) | −0.47 (−0.14) | 1.09 |
| 1/80 | 0.040 | 0.035 | 8.05 | −1.14 (−0.94) | 0.19 (0.34) | 0.19 (0.13) | −0.43 (−0.11) | 1.14 |
| Standard error in computed velocity coefficients: | | | ±0.03 | ±0.17 | ±0.29 | ±0.23 | ±0.21 | |

(1) Parameters ($Q/\phi_0$) used in equation (4).
(2) These coefficients correspond to those in equation (1); the values in brackets are the theoretical values of the coefficients.
(3) Model value 8.1 km/s.

**Table 4.** Western United States: summary of model studies for MOZAIC B.07.

| Model[1] ($Q/\phi_0$) | Uniform velocity solution variance ($s^2$) | Variance ($s^2$) | $V_0$[3] | General anisotropy solutions: computed velocity coefficients[2] $B$ | $C$ | $E$ | $F$ | $F$ ratio |
|---|---|---|---|---|---|---|---|---|
| 4/0 | 0.090 | 0.037 | 8.09 | 4.25 (4.00) | 0.35 (0.00) | 0.56 (0.67) | −0.08 (0.00) | 2.43 |
| 4/20 | 0.075 | 0.037 | 8.09 | 3.34 (3.06) | 2.88 (2.57) | 0.06 (0.12) | 0.49 (0.66) | 2.03 |
| 4/40 | 0.064 | 0.037 | 8.09 | 1.01 (0.69) | 4.23 (3.94) | −0.62 (−0.63) | 0.12 (0.23) | 1.73 |
| 4/60 | 0.072 | 0.037 | 8.09 | −1.66 (−2.00) | 3.76 (3.46) | −0.36 (−0.33) | −0.60 (−0.58) | 1.95 |
| 4/80 | 0.079 | 0.037 | 8.09 | −3.36 (−3.76) | 1.71 (1.37) | 0.40 (0.51) | −0.48 (−0.43) | 2.14 |
| 2/0 | 0.052 | 0.037 | 8.09 | 2.29 (2.00) | 0.36 (0.00) | 0.27 (0.33) | −0.09 (0.00) | 1.41 |
| 2/20 | 0.048 | 0.037 | 8.09 | 1.84 (1.53) | 1.62 (1.29) | 0.01 (0.06) | 0.22 (0.33) | 1.30 |
| 2/40 | 0.045 | 0.037 | 8.09 | 0.67 (0.35) | 2.30 (1.97) | −0.34 (−0.31) | 0.02 (0.11) | 1.22 |
| 2/60 | 0.046 | 0.037 | 8.09 | −0.67 (−1.00) | 2.06 (1.73) | −0.21 (−0.17) | −0.36 (−0.29) | 1.24 |
| 2/80 | 0.047 | 0.037 | 8.09 | −1.53 (−1.88) | 1.04 (0.68) | 0.19 (0.26) | −0.29 (−0.21) | 1.27 |
| 1/0 | 0.042 | 0.037 | 8.09 | 1.31 (1.00) | 0.36 (0.00) | 0.12 (0.17) | −0.09 (0.00) | 1.14 |
| 1/20 | 0.041 | 0.037 | 8.09 | 1.08 (0.77) | 0.99 (0.64) | −0.02 (0.03) | 0.07 (0.16) | 1.11 |
| 1/40 | 0.040 | 0.037 | 8.09 | 0.50 (0.17) | 1.33 (0.98) | −0.20 (−0.16) | −0.03 (0.06) | 1.08 |
| 1/60 | 0.040 | 0.037 | 8.09 | −0.17 (−0.50) | 1.21 (0.87) | −0.13 (−0.08) | −0.23 (−0.14) | 1.08 |
| 1/80 | 0.039 | 0.037 | 8.09 | −0.60 (−0.94) | −0.70 (0.34) | 0.07 (0.13) | −0.19 (−0.11) | 1.05 |
| Standard error in computed velocity coefficients: | | | ±0.02 | ±0.18 | ±0.29 | ±0.23 | ±0.26 | |

(1) Parameters ($Q/\phi_0$) used in equation (4).
(2) These coefficients correspond to those in equation (1): the values in brackets are the theoretical values of the coefficients.
(3) Model value 8.1 km/s.

and to the west of the Fault (Peake & Healy 1977). On the other hand, shots fired to the west of the Fault and observed to the east (shotpoints 1, 3 and 4 – Fig. 9) were retained because only a small part of the corresponding ray path actually lies to the west of the Fault; Bamford (1971) has shown that in such circumstances the error in travel time will be small, have negligible effects on the main velocity determination (here *east* of the Fault) and will simply be reflected as a systematically incorrect delay time computed for the shotpoint.

The working data set is thus based on the shots and stations shown in Fig. 13 and has the azimuthal distribution of observations shown in Fig. 12(b). For the purpose of anisotropy studies, the most effective part of the network is that in the Sierra Nevada where several profiles are reversed and intersect, and where much of the additional data at scattered stations are located. Model studies, based on two of the MOZAICs used for the analysis of the real data, are summarized in Tables 3 and 4. The 'measurement errors' alone should result in a variance of about 0.035 and 0.037 $s^2$ respectively and the critical $F$ ratio for significance at the 95 per cent confidence level is again about 1.16. The model studies indicate that the strength of the network depends on the direction of symmetry of the model anisotropy: in particular, the $F$ ratios are lowest when the maximum velocity is in the 40° direction, corresponding to the gap in the azimuth distribution (Fig. 12(b)). In general, however, an anisotropy at or above the 3 per cent level could be detected using the $F$ test and the velocity coefficients of the $2\phi$ terms remain well determined even at the 1.5 per cent level. This suggests that the combined use of time-term solutions and velocity scattergrams would here allow a reasonable opportunity of detecting any significant anisotropy present.

### 5.2 RESULTS

Four different MOZAIC studies, based on gravity, tectonic and basement maps of the western United States, have been attempted with the working data set. In the design of these MOZAICs the ancillary information was used to guess at the distribution of areas of equal delay time while keeping these areas reasonably small, say not greater than 20–50 km square. Thus all of the working data set could not always be incorporated into a particular MOZAIC. As an example, a MOZAIC based on tectonics is shown in Fig. 13 – it incorporates 534 travel-time observations distributed over 116 sites with the azimuthal distribution shown in Fig. 12(b). In general the MOZAICs were satisfactory from the point of giving stable solutions etc. although this stability depended to a certain extent upon the inclusion of the data that had been obtained from the literature.

The results obtained with the four MOZAICs, two based on gravity (G50 and G20, using gravity maps contoured at 50 and 20 milligal intervals, respectively), one on tectonics (T) and one on basement (B), are summarized in Table 5. In each case, the $F$ ratio is equal to or larger than that required for the inclusion of anisotropy to be significant at the 95 per cent confidence level. Furthermore in each case the final velocity scattergrams (Fig. 14) show visible evidence of velocity anisotropy and formal comparisons of uniform velocity and anisotropic fits (equation (1)) through the corresponding velocity–azimuth data indicate a significant azimuthal dependence ($F$ ratios between 1.44 and 1.94). However, it is clear from the fitted curves shown in Fig. 14 that the uneven distribution of observations as a function of azimuth has an important influence on these curves. In particular the gap in observations around 40° results in the $4\phi$ terms in equation (1) being rather poorly constrained – this shows up in the differences between the curves obtained when these terms are either excluded or included. We conclude that with this data set the most reliable

**Table 5.** Western United States: summary of results.

| MOZAIC | Number of observations used | Uniform velocity solution variance ($s^2$) | Variance ($s^2$) | General anisotropy solutions: computed velocity coefficients[1] | | | | | |
|---|---|---|---|---|---|---|---|---|---|
| | | | | $V_0$ | $B$ | $C$ | $E$ | $F$ | $F$ ratio |
| T.07 | 534 | 0.050 | 0.043 | 7.76 ± 0.03 | −1.11 ± 0.17 | 1.13 ± 0.23 | 0.49 ± 0.23 | 0.39 ± 0.21 | 1.16 |
| G50.07 | 520 | 0.053 | 0.043 | 7.75 ± 0.03 | −1.17 ± 0.16 | 1.21 ± 0.27 | 0.24 ± 0.21 | 0.57 ± 0.23 | 1.23 |
| B.07 | 534 | 0.043 | 0.037 | 7.77 ± 0.02 | −0.90 ± 0.16 | 1.04 ± 0.25 | −0.24 ± 0.20 | 0.88 ± 0.23 | 1.16 |
| G20.08 | 519 | 0.049 | 0.035 | 7.77 ± 0.02 | −1.40 ± 0.15 | 1.04 ± 0.25 | −0.09 ± 0.19 | 0.85 ± 0.22 | 1.40 |

(1) These coefficients correspond to those in equation (1).

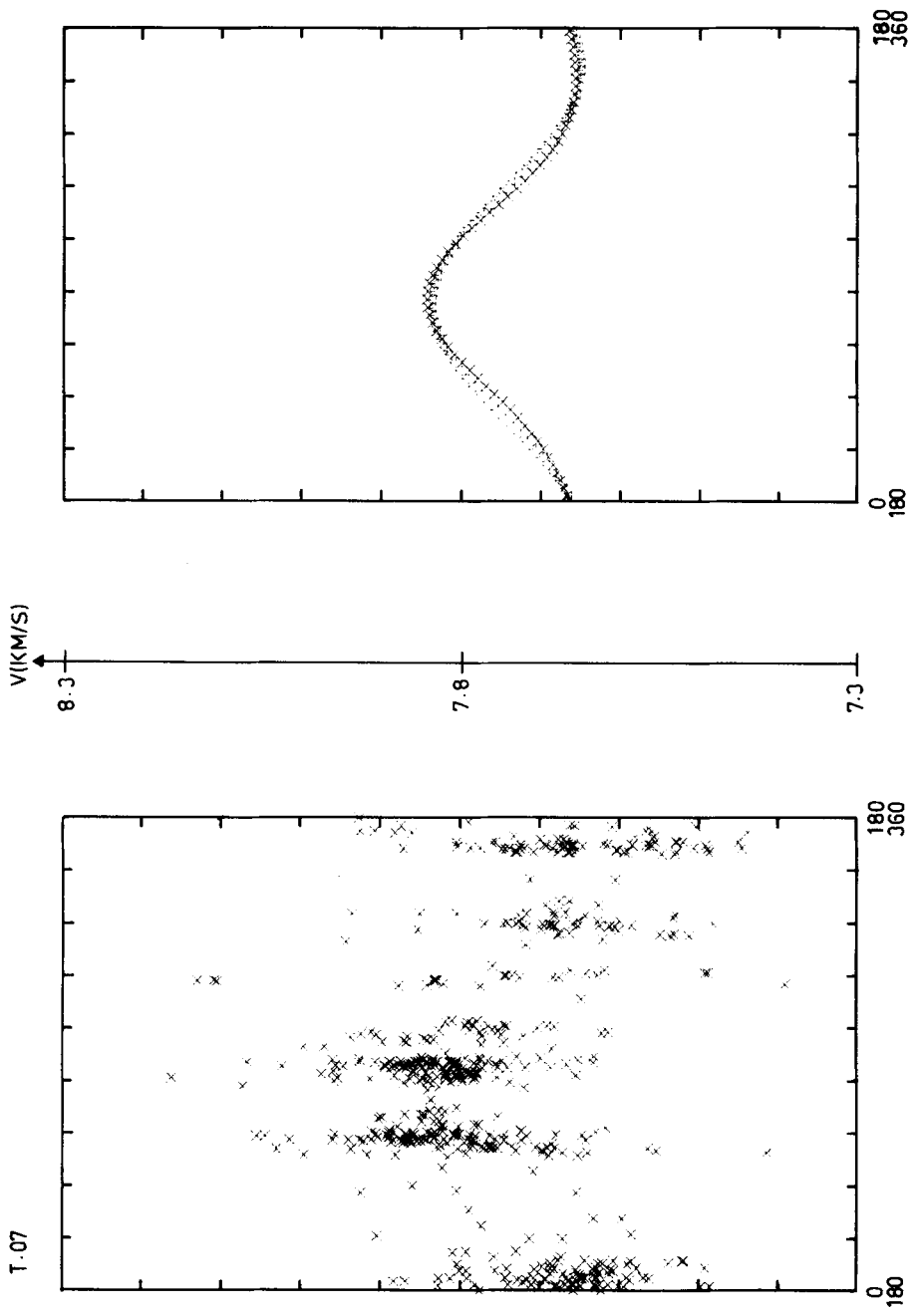


**Figure 14.** Velocity scattergrams, and fitted curves ($\Delta - 2\phi$ fit; $\times - 4\phi$ fit), for MOZAICs: (a) T.07, (b) B.07, (c) G50.07 and (d) G20.08; velocity ($V$) versus azimuth ($\phi$).

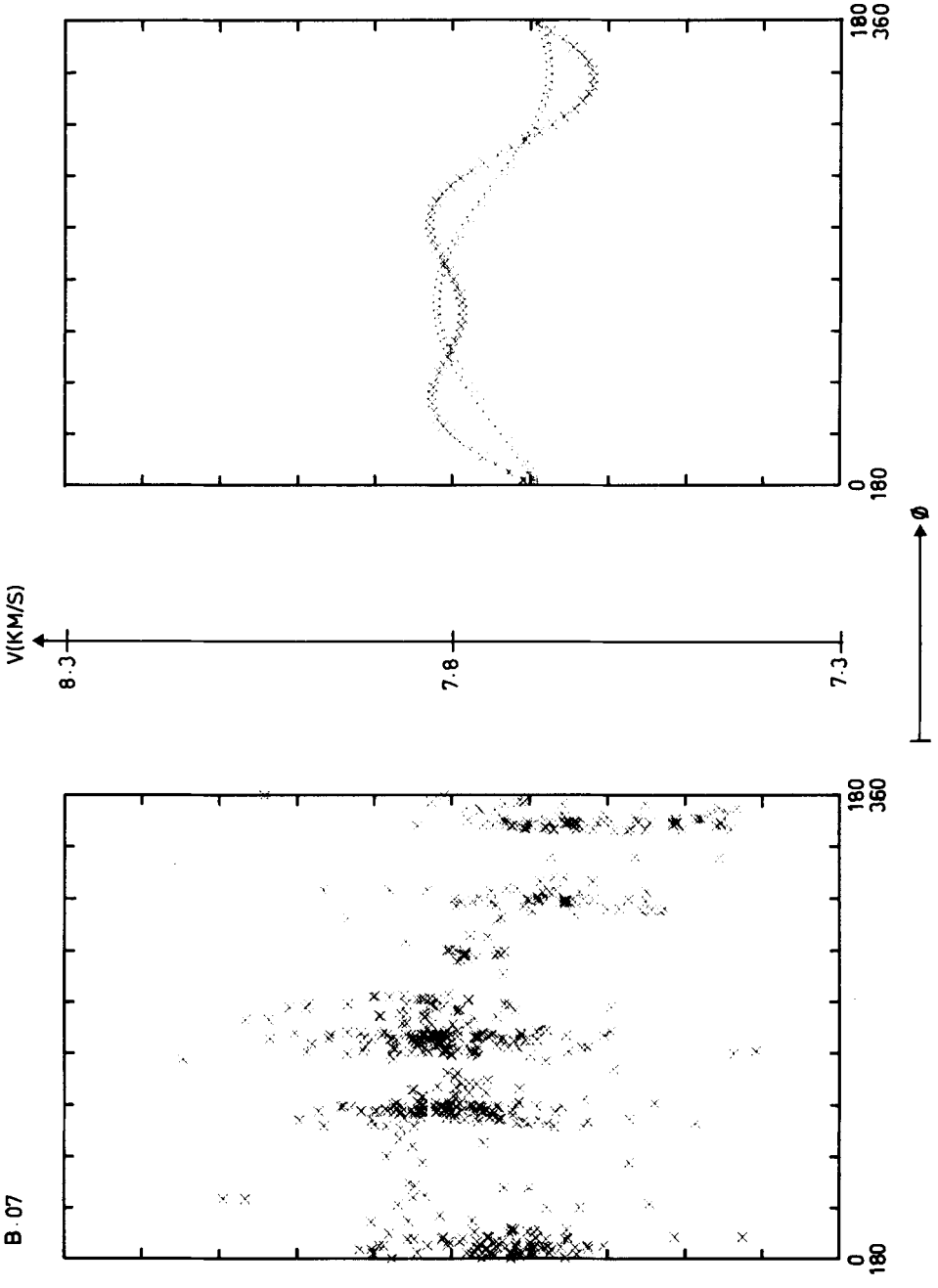


Figure 14 (b)

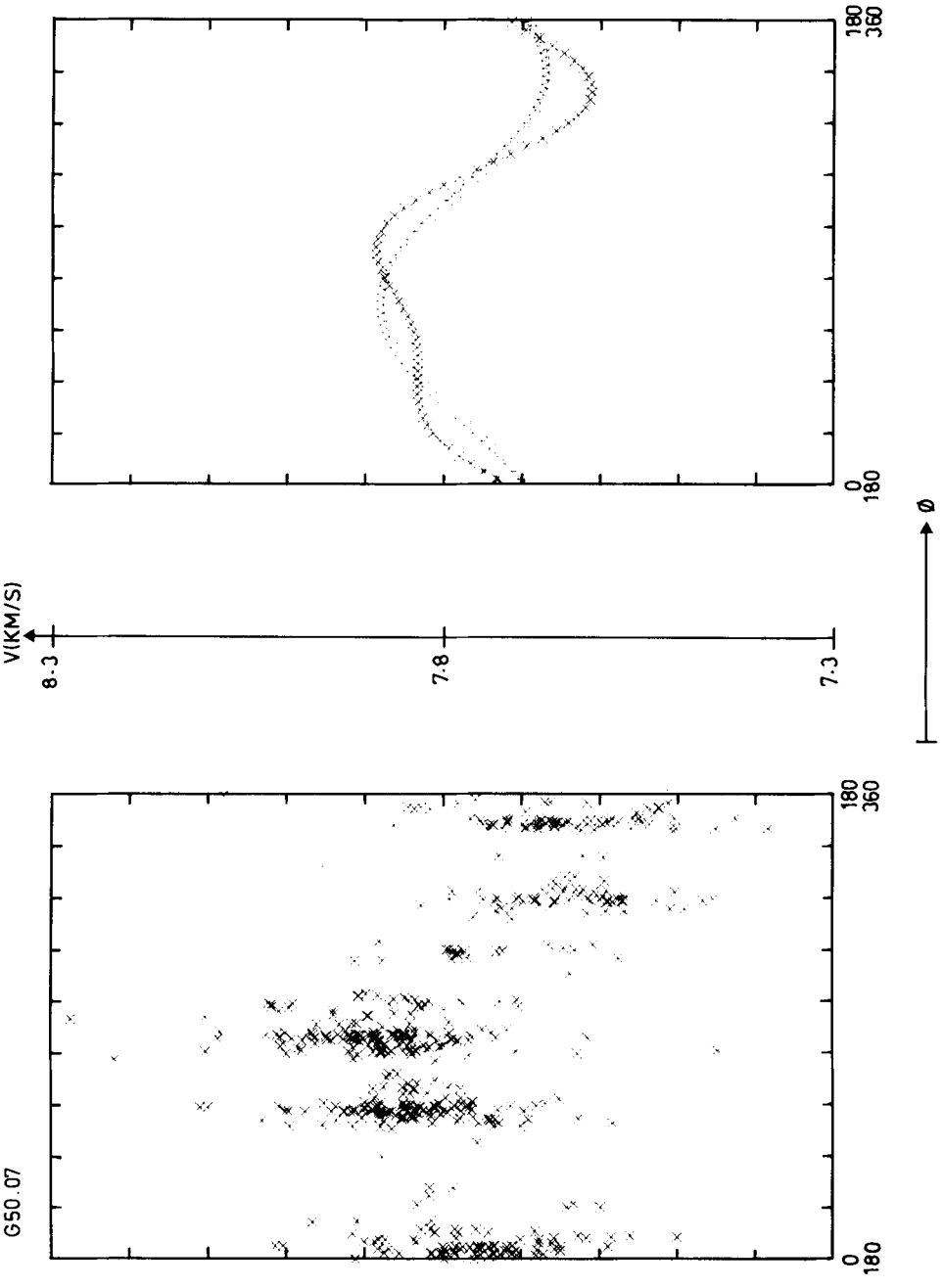


Figure 14 (c)

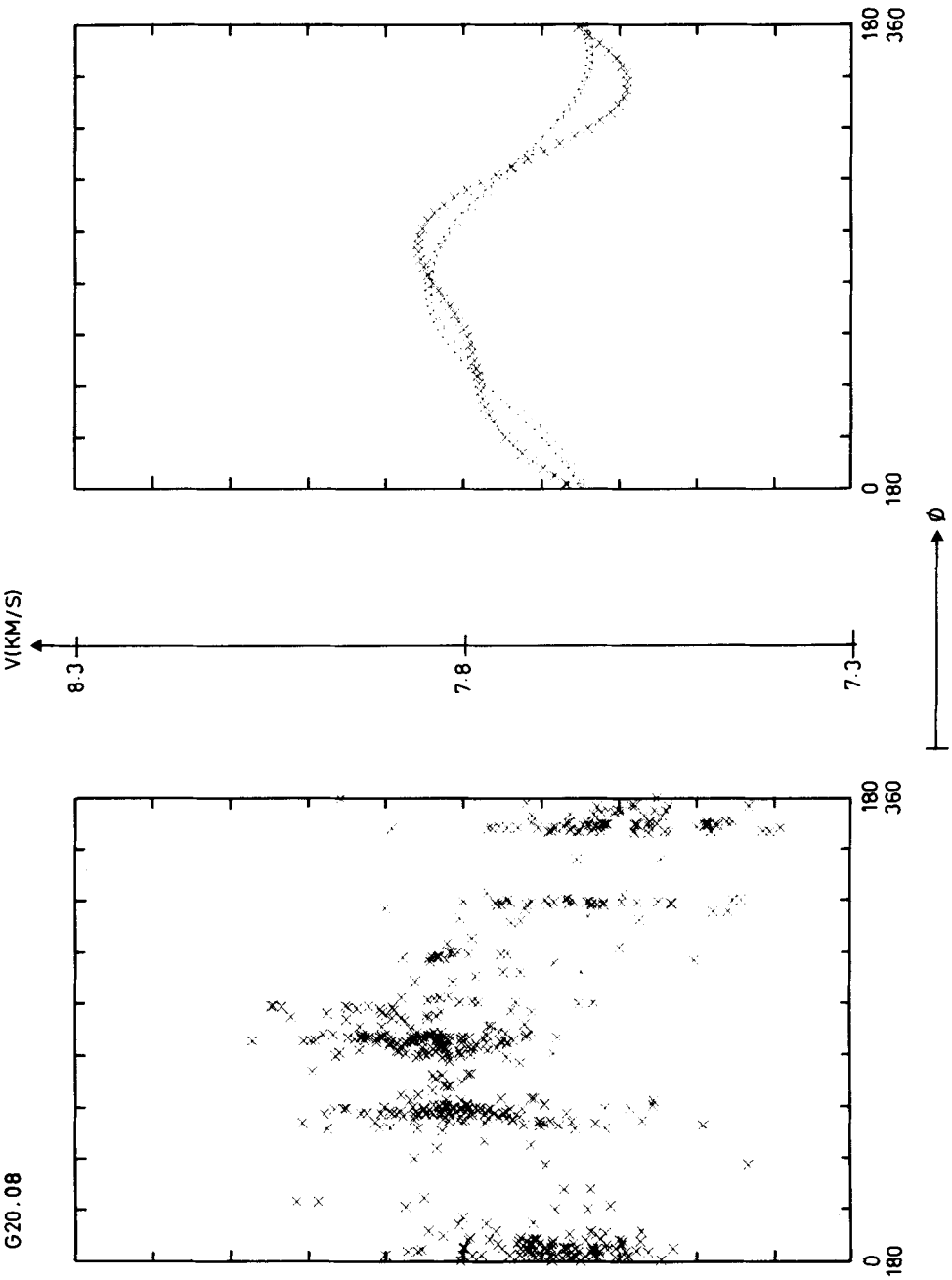


Figure 14 (d)

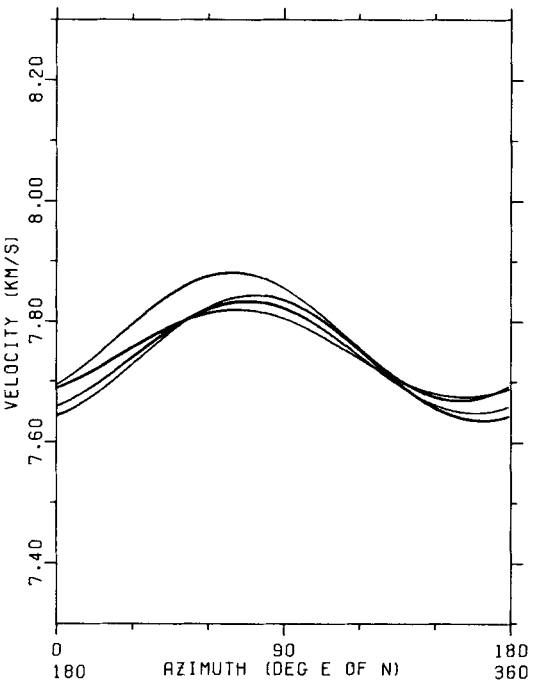


**Figure 15.** Compilation of velocity–anisotropy curves ($2\phi$ fits) for MOZAICs T.07, B.07, G50.07 and G20.08: velocity ($V$) versus azimuth ($\phi$). In each case, two separate curves are shown (one for all data, the other for observation distance less than 300 km) – they are more or less indistinguishable.

results will be those based on curves in which *only* the $2\phi$ terms are included. Fig. 15 summarizes these curves for the four MOZAICs studied: since the data beyond 300 km are those over which the authors have least control, they being mainly derived from the literature, two curves are plotted in each case, the first fitted through all observations, the second only through observations at distances less than 300 km – the differences are in fact negligible.

Fig. 15 suggests that the data are consistent with the presence of an anisotropy of 2–3 per cent with the maximum velocity (> 7.8 km/s) in a direction 70–80° east of north. In order to check that this is not simply an *apparent* anisotropy resulting from the coincidental sampling of a laterally varying refractor velocity, values used in one of the better velocity scattergrams (T.07, Fig. 14(a)) have been plotted as a function of position. In an attempt to overcome the inherent scatter of the velocity values, each one has been graded according to a simple scheme and then plotted mid-way between the corresponding shotpoint and station – itself a considerable approximation as the value is in reality an average for the whole path. The result is shown in Fig. 16. There appears to be no pattern, corresponding to a lateral variation in refractor velocity, which could lead to an apparent anisotropy with a minimum velocity less than 7.7 km/s (grade *C*) and a maximum greater than 7.8 km/s (grade *E*).

## 6 Discussion

In none of the cases studied are the data ideally suited to the detection and measurement of $P_n$ velocity anisotropy. While that for the eastern United States is clearly the least satis-

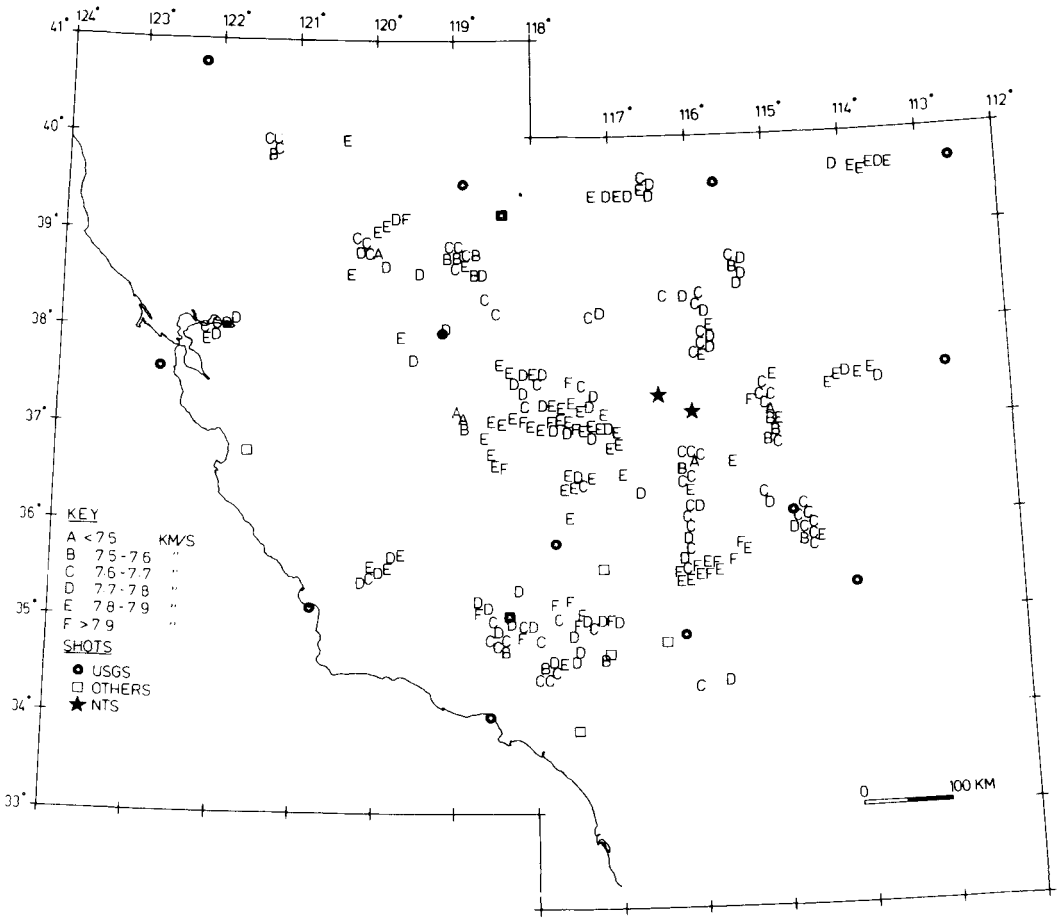


**Figure 16.** Velocity values, graded and plotted as a function of position, western United States.

factory of the three in nearly every respect, the geographic and azimuthal distributions of the observations in both northern Britain and the western United States are less satisfactory than those used in other anisotropy studies, for example in the Pacific Ocean by Raitt *et al.* (1969) and Morris *et al.* (1969), in western Germany by Bamford (1977) and in near-surface studies by Bamford & Nunn (1978). This is an important consideration when assessing the significance of the results we have obtained: nevertheless we suggest that their broad aspects are not primarily controlled by the data quality. Specifically, within the error limits of the available data, the uppermost mantle appears to be isotropic under northern Britain and the eastern United States, but shows a small but significant anisotropy in the western United States. The scatter in the velocity values (Figs 14 and 15) precludes any inversion of the anisotropy observed beneath the western United States into a petrological structure using the methods devised by Crampin & Bamford (1977) for the Pacific Ocean and west German observations. We concentrate only on the broader aspects of our result, namely the amount (2–3 per cent) and direction (70–80° east of north) of the anisotropy.

Peselnick *et al.* (1977) have measured the anisotropic elastic velocities of two lherzolite xenoliths derived from the upper mantle beneath the Sierra Nevada batholith and calculated, at the temperatures and pressures likely *in situ*, maximum and minimum velocities of

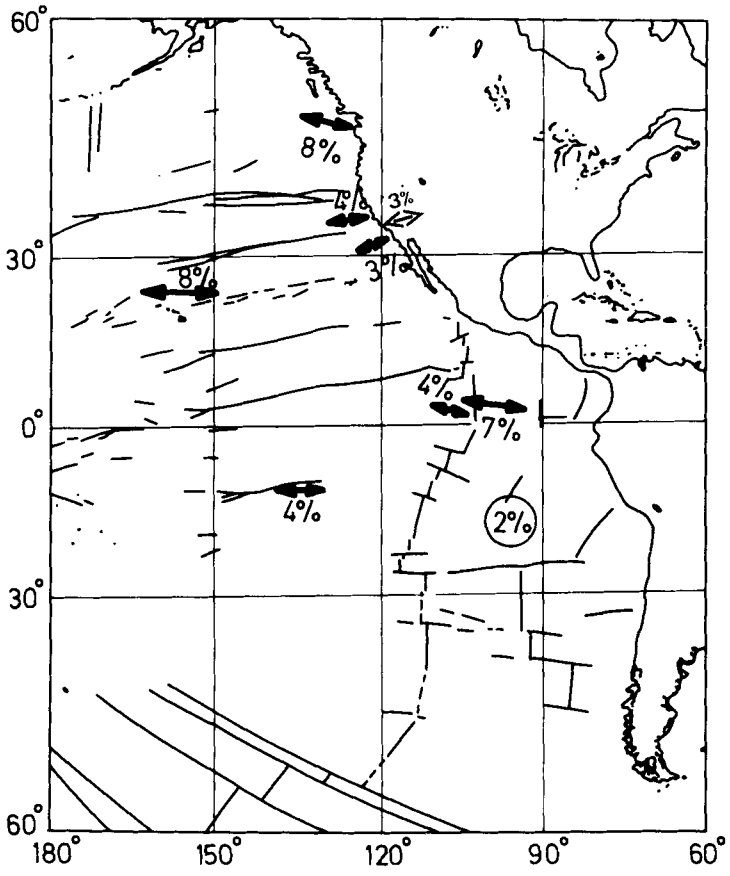


**Figure 17.** Compilation of $P_n$ velocity anisotropy results for the western United States (this study) and the north-eastern Pacific: this map is a modified version of fig. 4 of Fuchs (1977) which was in turn based on fig. 14 of Raitt *et al.* (1971).

8.4 ± 0.1 and 7.85 ± 0.12 km/s respectively. It is probable that their results relate to a somewhat greater depth than the immediate sub-Moho sampled by $P_n$ refraction studies: this would explain the difference in the amount of anisotropy between our results and theirs. Peselnick *et al.* suggested that *in situ* their anisotropy might have the same direction as that found in the adjacent ocean. In Fig. 17 we show our result plotted together with published results for the north-eastern Pacific – remarkably both the amount and the direction of the anisotropy beneath the western United States are very similar to those found in the Pacific Ocean off California by Raitt *et al.* (1969).

We regard this similarity as a reflection of the intimate dependence of the tectonic evolution of the western United States upon the presence of nearby ocean and concur with Peselnick *et al.* who suggest that the existence of large-scale upper mantle anisotropy in that area is possibly a consequence of the subduction of oceanic lithosphere during Mesozoic time (Hamilton 1969). In particular, we note that if, as Snyder, Dickinson & Silberman (1976) suggest, in late Mesozoic and Oligocene times a series of magmatic arcs extended parallel to the continental margin from Canada to Mexico, back-arc extension and high temperatures could have effected broad regions of the continental edge at that time. This combination would have allowed upper mantle anisotropy to develop there in the direction

of tension, in this case in the direction of spreading of the adjacent ocean. A similar process may have operated in the Sea of Japan, for example, which has extended, still has generally high heat flow (Uyeda 1977), and in which an upper mantle anisotropy of several per cent has been measured (Asano 1977, private communication) with the maximum velocity in the direction of extension.

The apparent absence of upper mantle anisotropy in northern Britain and the eastern United States, if confirmed by future and better measurements, could simply reflect a different tectonic style. Both are regions of ancient collision orogeny (Caledonian) and are currently adjacent to passive continental margins. It may be that conditions to create such large-scale anisotropy have never existed there or that an ancient anisotropy was destroyed by subsequent tectonic events.

Clearly this subject is a field where a lot of speculation regarding tectonics, petrology etc. is possible. However, the results obtained in the western United States are not good enough to support detailed petrologic models of that area and not enough continental areas have yet been studied to allow broad tectonic conclusions based on the presence/absence of anisotropy in the uppermost mantle. The prime requirement is therefore for extended studies, possibly using a variety of data, in the western United States, and for further studies of the type undertaken here in other continental areas.



## Acknowledgments

The authors are indebted to Karl Fuchs, Stuart Crampin, Sonja Faber and Gerhard Müller for their critical comments on a first draft of this paper.

The original, and unpublished, data for the record sections from the western United States used in this study were provided by the National Center for Earthquake Research of the United States Geological Survey, Menlo Park, California during an appointment of one of the authors (CP) as a Visiting Scientist. Computing facilities were made available by both the Geophysical Institute and the Computing Centre of the University of Karlsruhe.

We are indebted to Ingrid Hörnchen for typing the manuscript. Contribution No. 156, University of Karlsruhe.

## References

Allen, C. R. & Helmberger, D. V., 1973. Search for temporal changes in seismic velocities using large explosions in southern California, *Proceedings of Conference on Tectonic Problems of the San Andreas Fault System*, pp. 436–445, eds Kovach, R. B. & Nur, A., Stanford University.

Backus, G. E., 1965. Possible forms of seismic anisotropy of the uppermost mantle under oceans, *J. geophys. Res.*, **70**, 3429–3439.

Bamford, D., 1971. Applications of simulated data studies to crustal refraction seismology, *Bull. seism. Soc. Am.*, **61**, 1013–1032.

Bamford, D., 1973. Refraction data in Western Germany – a time-term interpretation, *Z. Geophys.*, **39**, 907–927.

Bamford, D., 1976. MOZAIC time-term analysis, *Geophys. J. R. astr. Soc.*, **44**, 433–446.

Bamford, D., 1977. $P_n$ velocity anisotropy in a continental upper mantle, *Geophys. J. R. astr. Soc.*, **49**, 29–48.

Bamford, D. & Crampin, S., 1977. Seismic anisotropy – the state of the art, *Geophys. J. R. astr. Soc.*, **49**, 1–8.

Bamford, D. & Nunn, K., 1978. *In situ* seismic measurements of crack anisotropy in the carboniferous limestone of northwest England, *Geophys. Prosp.*, in press.

Bamford, D., Nunn, K., Prodehl, C. & Jacob, B., 1978. LISPB IV – Crustal structure of Northern Britain, *Geophys. J. R. astr. Soc.*, **54**, 43–60.

Bibee, L. D. & Shor, G. G., 1976. Compressional wave anisotropy in the crust and upper mantle, *Geophys. Res. Lett.*, **3**, 639–642.

Borcherdt, R. D. & Roller, J. C., 1966. A preliminary summary of a seismic-refraction survey in the vicinity of the Cumberland Plateau Observatory, Tennessee, *U.S. Geo. Surv., Tech. Lett. No. 43.*

Carder, D. S., 1973. Trans-California seismic profile. Death Valley to Monterey Bay, *Bull. seism. Soc. Am.*, **63**, 571–586.

Carder, D. S., Qamar, A. & McEvilly, T. V., 1970. Trans-California seismic profile – Pahute Mesa to San Francisco Bay, *Bull. seism. Soc. Am.*, **60**, 1829–1846.

Crampin, S., 1977a. Palaeoanisotropy in the upper mantle, *Nature*, **270**, 162–163.

Crampin, S., 1977b. A review of the effects of anisotropic layering on the propagation of seismic waves, *Geophys. J. R. astr. Soc.*, **49**, 9–27.

Crampin, S. & Bamford, D., 1977. Inversion of *P*-wave velocity anisotropy, *Geophys. J. R. astr. Soc.*, **49**, 123–132.

Davies, O. L., 1961. *Statistical Methods in Research and Production*, 3rd edn, Oliver & Boyd, Edinburgh.

Fuchs, K., 1977. Seismic anisotropy of the subcrustal lithosphere as evidence for dynamical processes in the upper mantle, *Geophys. J. R. astr. Soc.*, **49**, 167–179.

Hales, A. L., Helsey, C. E., Dowling, J. J. & Nation, J. B., 1968. The East Coast Onshore–Offshore Experiment, I. The first arrival phases, *Bull. seism. Soc. Am.*, **58**, 757–819.

Hamilton, W. B., 1969. Mesozoic California and the underflow of Pacific mantle, *Bull. geol. Soc. Am.*, **80**, 2409–2430.

Jacob, B., 1975. The Scottish seismic refraction programme, *Proc. XIII Assem. European Seism. Comm. (Brasov 1972)*, pp. 325–328.

Jacob, B. & Willmore, P., 1975. 10 ton explosions fired in 1971 and 1972, *Proc. XIII Assem. European Seism. Comm. (Brasov 1972)*, pp. 329–337.

James, D. E., Smith, T. J. & Steinhart, J. S., 1968. Crustal structure of the Middle Atlantic States, *J. geophys. Res.*, **73**, 1983–2007.

Kanamori, H. & Fuis, G., 1976. Variation of *P*-wave velocity before and after the Galway Lake earthquake and the Goat Mountain earthquakes, 1975, in the Mojave Desert, California, *Bull. seism. Soc. Am.*, **66**, 2017–2037.

Kanamori, H. & Hadley, D., 1975. Crustal structure and temporal velocity change in Southern California, *Pageoph.*, **113**, 257–280.

Kind, R., 1972. Residuals and velocities of $P_n$ waves recorded by the San Andreas seismograph network, *Bull. seism. Soc. Am.*, **62**, 85–100.

Lehmann, I., 1962. The travel times of the longitudinal waves of the LOGAN and BLANCA atomic explosions and their velocities in the upper mantle, *Bull seism. Soc. Am.*, **52**, 519–526.

Lewis, B. T. R. & Meyer, R. P., 1977. Upper mantle velocities under the East Coast margin of the U.S., *Geophys. Res. Lett.*, **4**, 341–344.

Mikumo, T., 1965. Crustal structure in central California in relation to the Sierra Nevada, *Bull. seism. Soc. Am.*, **55**, 65–83.

Morris, G. B., Raitt, R. W. & Shor, G. G., 1969. Velocity anisotropy and delay-time maps of the mantle near Hawaii, *J. geophys. Res.*, **74**, 4300–4316.

Peake, L. G. & Healy, J. H., 1977. A method for determination of the lower crustal structure along the San Andreas fault system in central California, *Bull. seism. Soc. Am.*, **67**, 793–807.

Peselnick, L., Lockwood, J. P. & Stewart, R., 1977. Anisotropic elastic velocities of some upper mantle Xenoliths underlying the Sierra Nevada batholith, *J. geophys. Res.*, **82**, 2005–2010.

Peselnick, L., Nicolas, A. & Stevenson, P. R., 1974. Velocity anisotropy in a mantle periodotite from the Ivrea Zone: application to upper mantle anisotropy, *J. geophys. Res.*, **79**, 1175–1182.

Prodehl, C., 1970a. Seismic refraction study of crustal structure in the western United States, *Bull geol. Soc. Am.*, **81**, 2629–2646.

Prodehl, C., 1970b. Crustal structure of the western United States from seismic-refraction measurements in comparison with central European results, *Z. Geophys.*, **36**, 477–500.

Prodehl, C., 1978. Crustal structure of the western United States, *U.S. Geol. Surv. Prof. Paper*, in press.

Raitt, R. W., Shor, G. G., Francis, T. J. G. & Morris, G. B., 1969. Anisotropy of the Pacific upper mantle, *J. geophys. Res.*, **74**, 3095–3109.

Raitt, R. W., Shor, G. G., Morris, G. B. & Kirk, H. K., 1971. Mantle anisotropy in the Pacific Ocean, *Tectonophys.*, **12**, 173–186.

Smith, P. J., 1975. *PhD thesis*, University of Durham.

Smith, P. J. & Bott, M. H. P., 1975. Structure of the crust beneath the Caledonian Foreland and Caledonian Belt of the North Scottish Shelf Region, *Geophys. J. R. astr. Soc.*, **40**, 187–205.

Snyder, W. S., Dickinson, W. R. & Silverman, M. L., 1976. Tectonic implications of space-time patterns of Cenozoic magmatism in the western United States, *Earth planet. Sci. Lett.*, **32**, 91–106.

Sornes, A., 1968. $P_n$ time-term survey Norway–Scotland 1969, ARPA No. 612–1, *Suppl. Sci. Rep.*

Uyeda, S., 1977. Some basic problems in the trench-arc-back arc system, *Island Arcs, Deep Sea Trenches and Back-Arc Basins,* pp. 1–14, eds Talwani, M. & Pitman III, W. C., A.G.U. Maurice Ewing Series 1.

Wesson, R. L., Roller, J. C. & Lee, W. H. K., 1973. Time-term analysis and geological interpretation of seismic travel-time data from the Coast Ranges of central California, *Bull. seism. Soc. Am.*, **63**, 1447–1471.